Blessed Plots for the Reversed Horn Current Analysis

J. Evans, J. Hartnell, A. Himmel and D. Naples
for the NuMuBar Group

April 2, 2011
Version 9
(minos-doc-7929-v9)

Document Versions

This document is intended to be a one stop shop that will always have the latest NuMuBar blessed plots in it for the reversed horn current analysis.

Version 1 (minos-doc-7929-v1): Copied over from minos-doc-6993-v18, but with final versions of the CC and NuBar results. Still missing are the Super-Kamiokande figures and updated future sensitivities.

Version 2 (minos-doc-7929-v2): Added updated SuperK plots.

Version 3 (minos-doc-7929-v3): Added future sensitivity plots.

Version 4 (minos-doc-7929-v4): Addressing comments from group blessing.

Version 5 (minos-doc-7929-v5): Revised many captions to remove jargon and improve clarity and accuracy. Added PRL plots along with their captions from the PRL at the end.

Version 6 (minos-doc-7929-v6): Fixed a typo in the SuperK legend.

Version 7 (minos-doc-7929-v7): Fixed some small mistakes in the event counts.

Version 8 (minos-doc-7929-v8): Further detailed study of the event counts showed that the previous results plots had been made with an obsolete best fit value. All results plots updated accordingly. Also added the combined significance to the slide with the oscillation results.

Version 9 (minos-doc-7929-v9): Updated future sensitivity plots.

Brief Overview

The goal of this analysis is to determine the spectrum of $\overline{\nu}_\mu$ events in the Far Detector that will be used to extract physics model parameters. The search for $\overline{\nu}_\mu$ disappearance constrains $\overline{\nu}_\mu \rightarrow \overline{\nu}_\tau$ oscillation parameters. In particular, $\overline{\nu}_\mu$ disappearance will constrain oscillation parameters $\Delta\overline{m}^2$ and $\sin^2(2\overline{\theta}_{23})$ through the measured oscillation probability,

$$P(\overline{\nu}_\mu \rightarrow \overline{\nu}_\mu) = 1 - \sin^2(2\overline{\theta}_{23}) \sin^2\left(1.27\Delta\overline{m}^2 \frac{L}{E}\right).$$

Selection Efficiency and Purity

minos-doc-6984

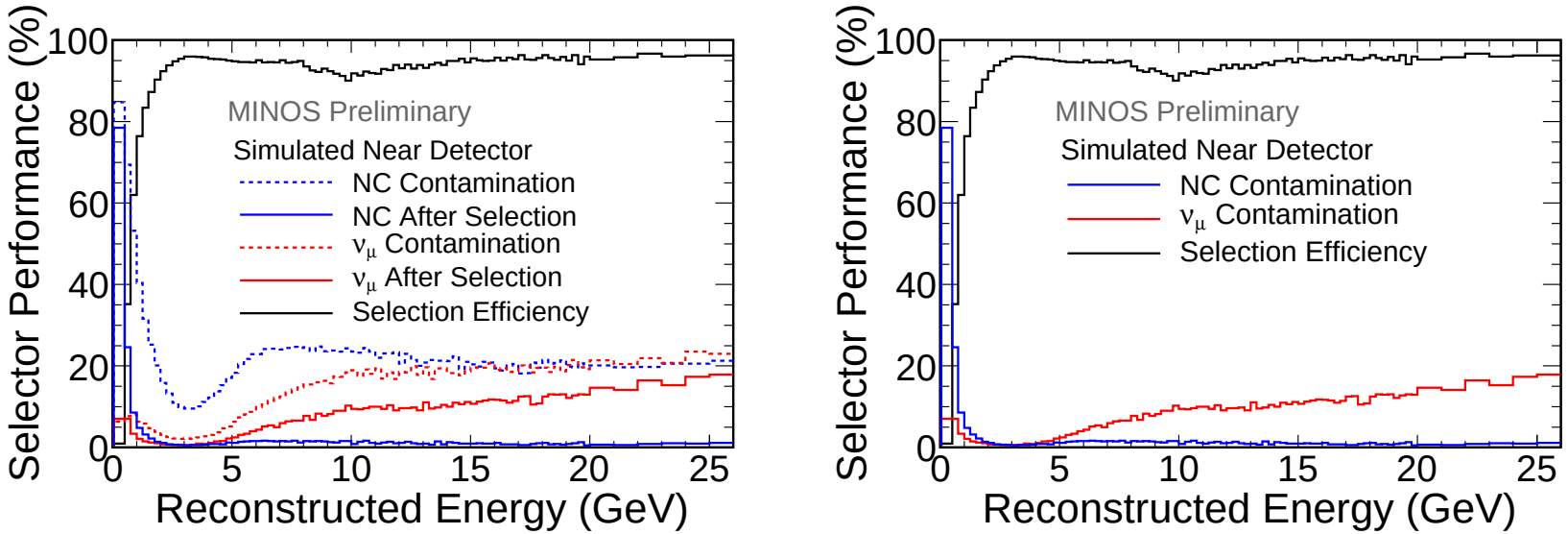

Figure 1: Performance of the RHC selection in the Near Detector (CC/NC separator > 0.3, positive reconstructed charge). The RHC selection is equivalent to the 2008 CC selection, but with the opposite charge sign selected. The dashed lines show the contamination before selection and the solid show efficiency and contamination after selection. The ν_μ contamination rises at higher energies since these tracks do not curve as much and so are more difficult to assign a charge to. minos-doc-6984

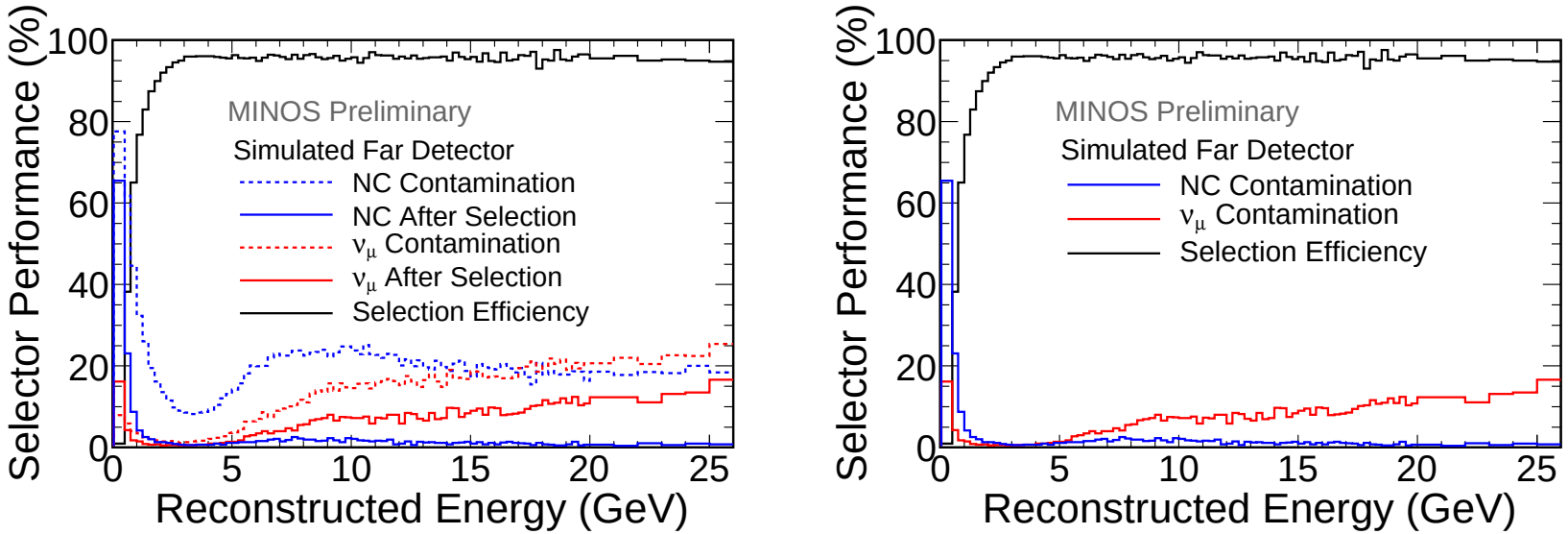

Figure 2: Performance of the RHC selection in the Far Detector (CC/NC separator > 0.3, positive reconstructed charge). The RHC selection is equivalent to the 2008 CC selection, but with the opposite charge sign selected. The dashed lines show the contamination before selection and the solid show efficiency and contamination after selection. The ν_μ contamination rises at higher energies since these tracks do not curve as much and so are more difficult to assign a charge to. minos-doc-6984

ND Data/MC distributions

minos-doc-7337

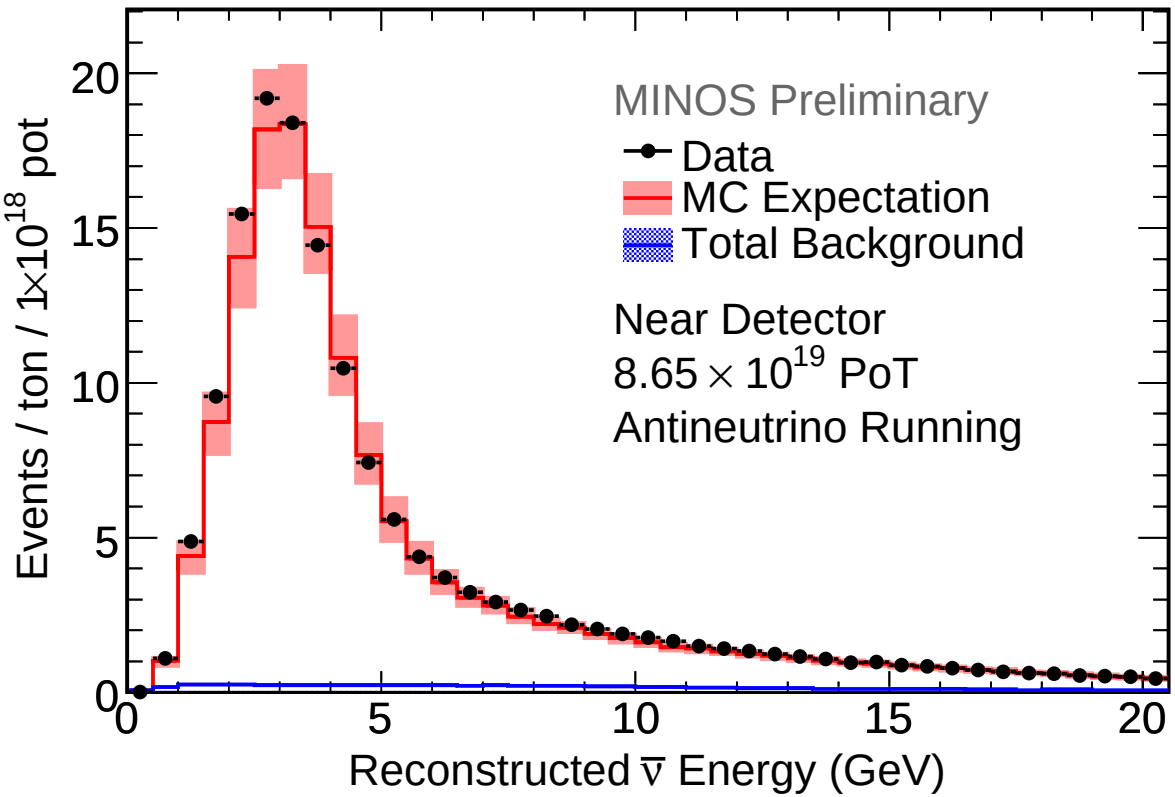

Figure 3: Reconstructed energy distribution of events selected as antineutrinos in the Near Detector. The red histogram represents the Monte Carlo expectation with the systematic error, the blue histogram represents the total (charged and neutral current) background with the background uncertaintiy. Black points represent data.

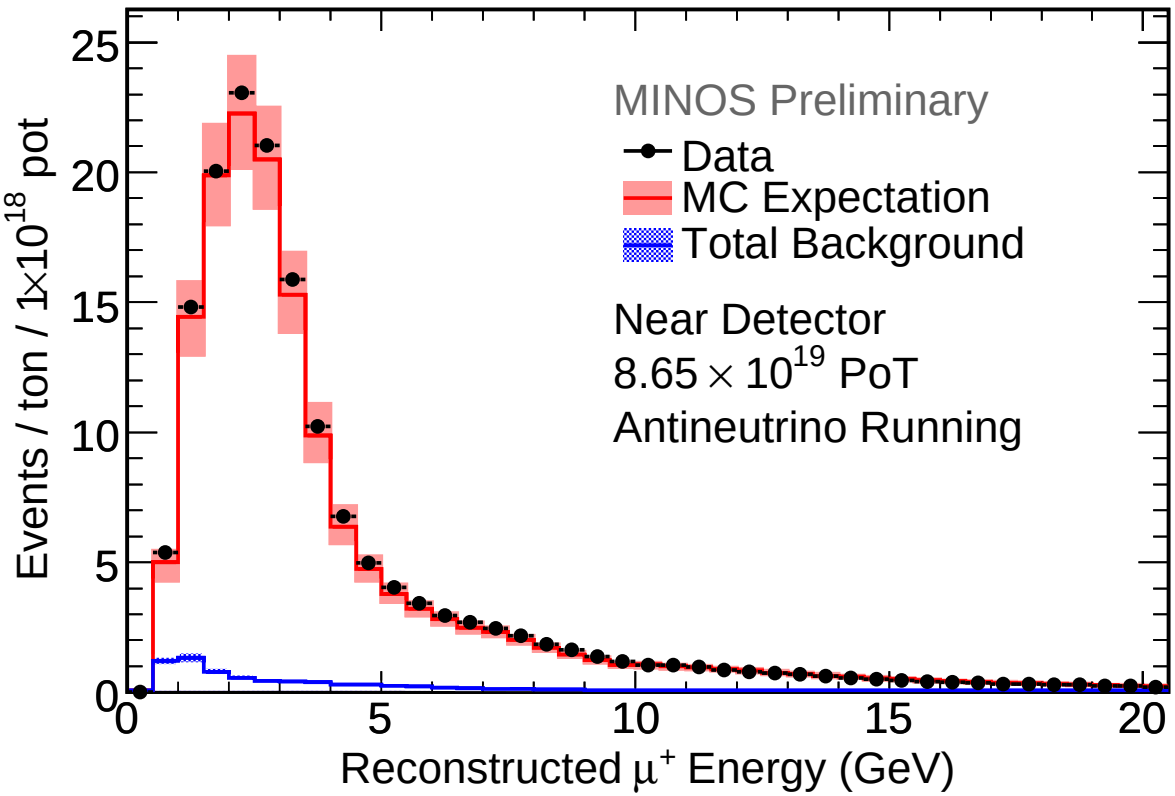

Figure 4: Reconstructed momentum of μ^+ tracks in the Near Detector. The red histogram represents the Monte Carlo expectation with the systematic error, the blue histogram represents the total (charged and neutral current) background with the background uncertaintiy. Black points represent data.

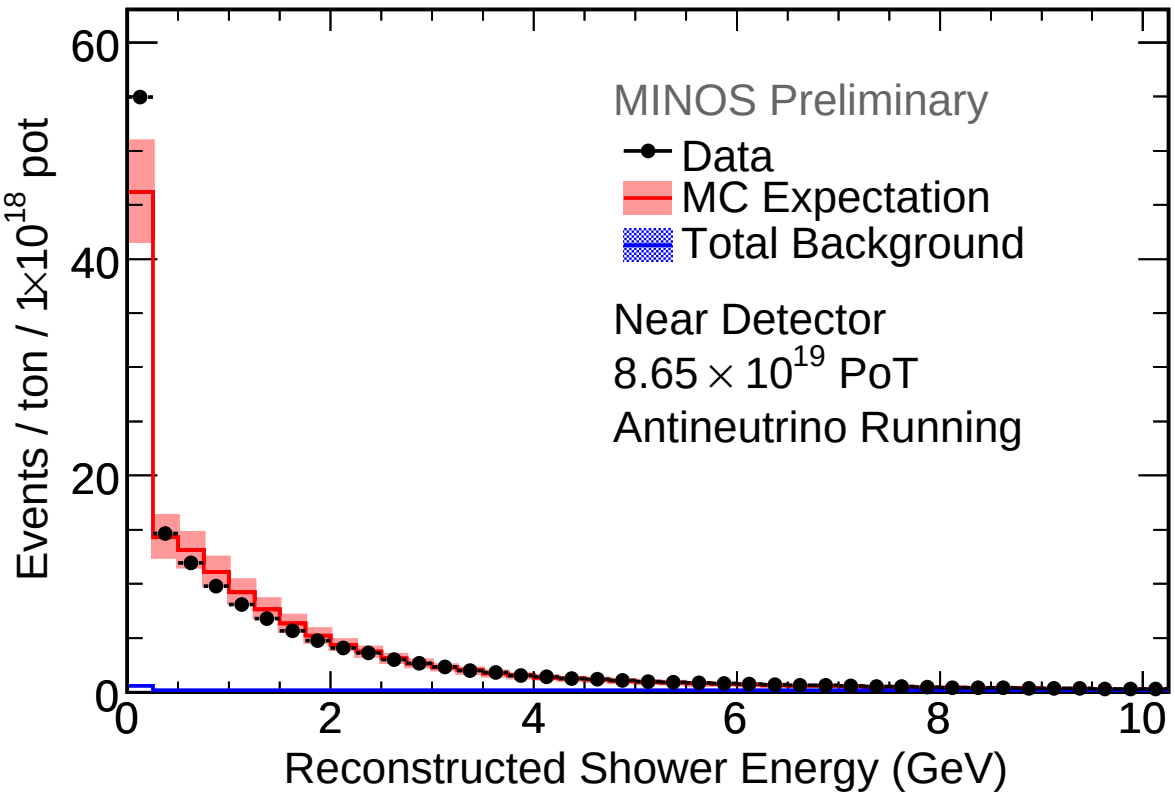

Figure 5: Reconstructed shower energy distribution of events selected as antineutrinos in the Near Detector. The red histogram represents the Monte Carlo expectation with the systematic error, the blue histogram represents the total (charged and neutral current) background with the background uncertaintiy. Black points represent data.

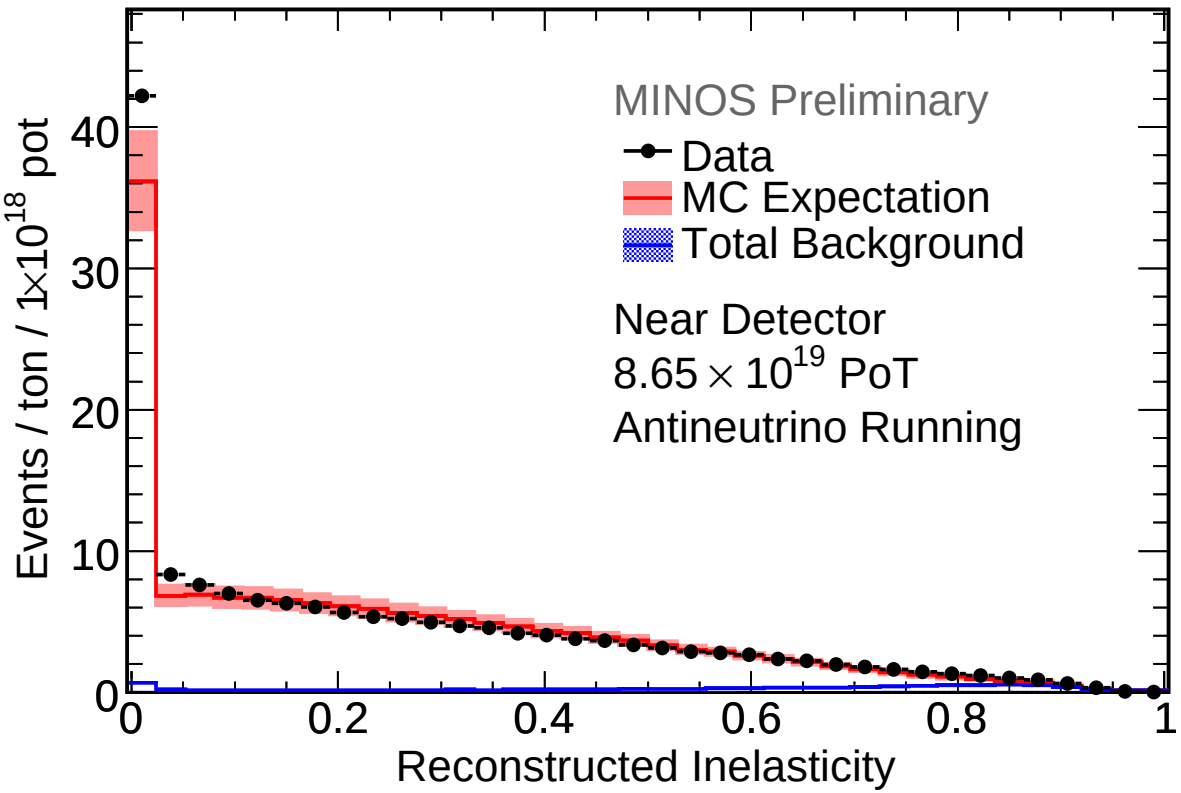

Figure 6: Reconstructed inelasticity distribution of events selected as antineutrinos in the Near Detector. The red histogram represents the Monte Carlo expectation with the systematic error, the blue histogram represents the total (charged and neutral current) background with the background uncertainty. Black points represent data.

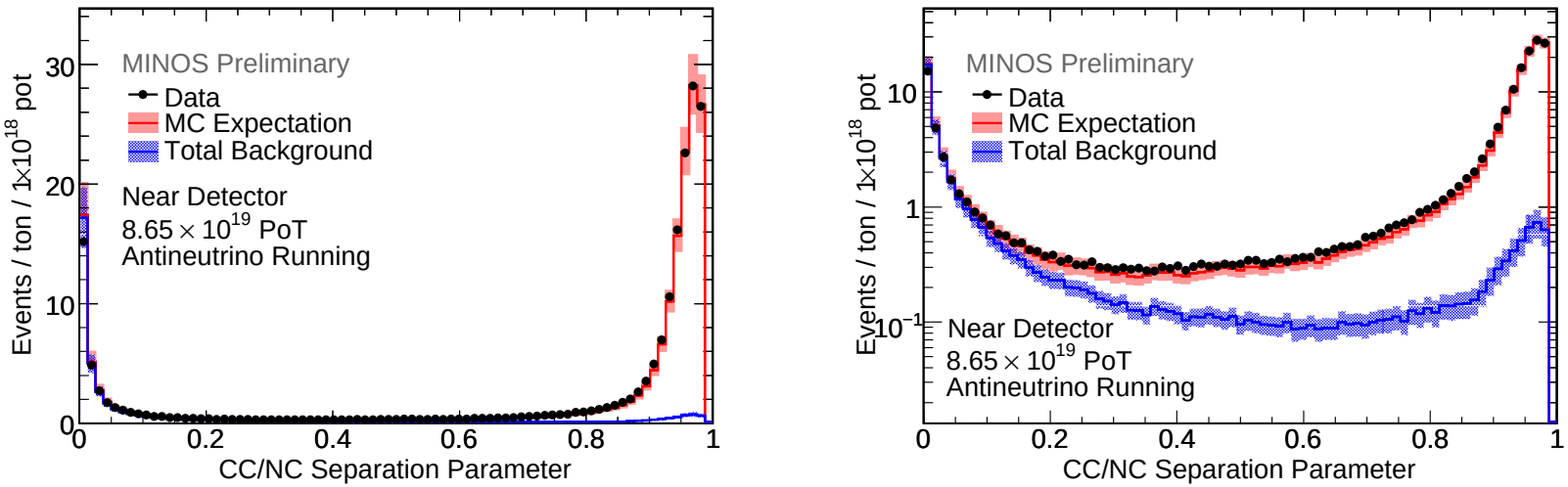

Figure 7: The CC/NC separation parameter (called $roID$ internally) in the Near Detector. The cut removes events below 0.3. This is the same CC/NC separation cut used in the 2008 CC analysis. The red histogram represents the Monte Carlo expectation with the systematic error, the blue histogram represents the total (charged and neutral current) background with the background uncertaintiy. Black points represent data.

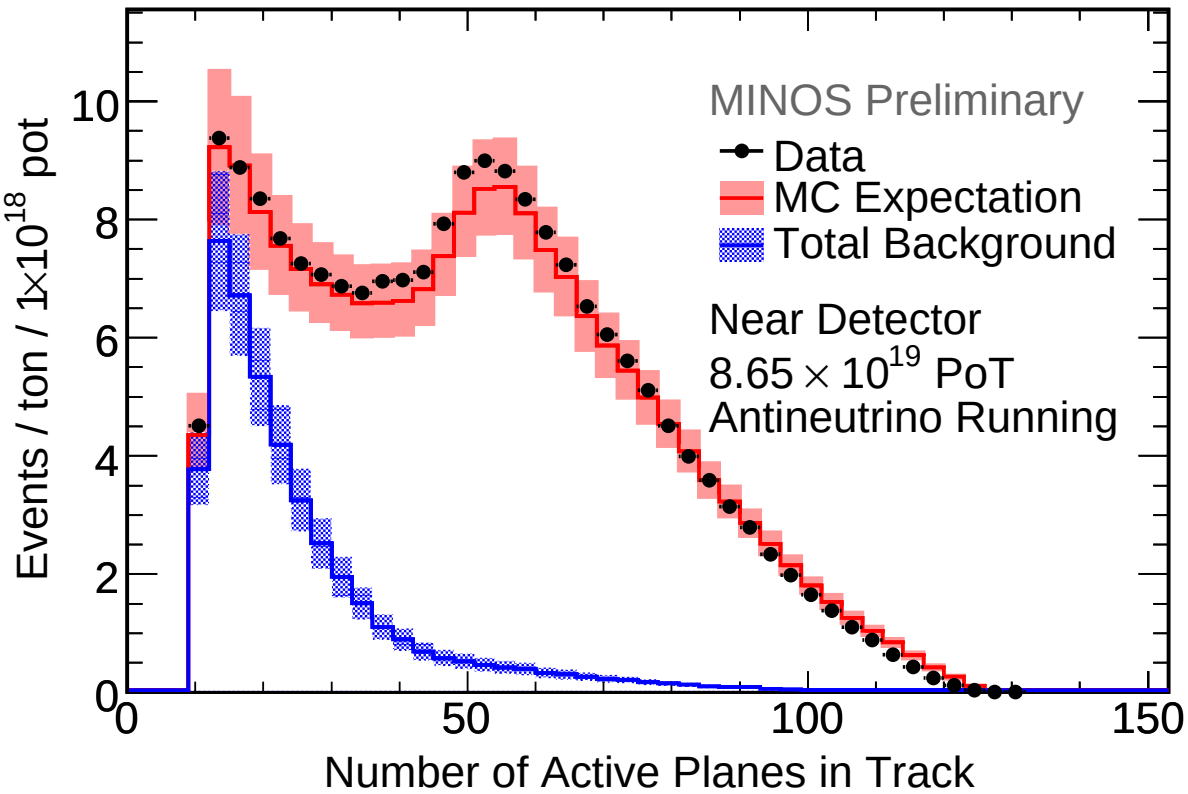

Figure 8: The number of active scintillator planes in the track, an input to the CC/NC separator, shown in the Near Detector before the CC/NC separation cut has been applied. The red histogram represents the Monte Carlo expectation with the systematic error, the blue histogram represents the total (charged and neutral current) background with the background uncertaintiy. Black points represent data.

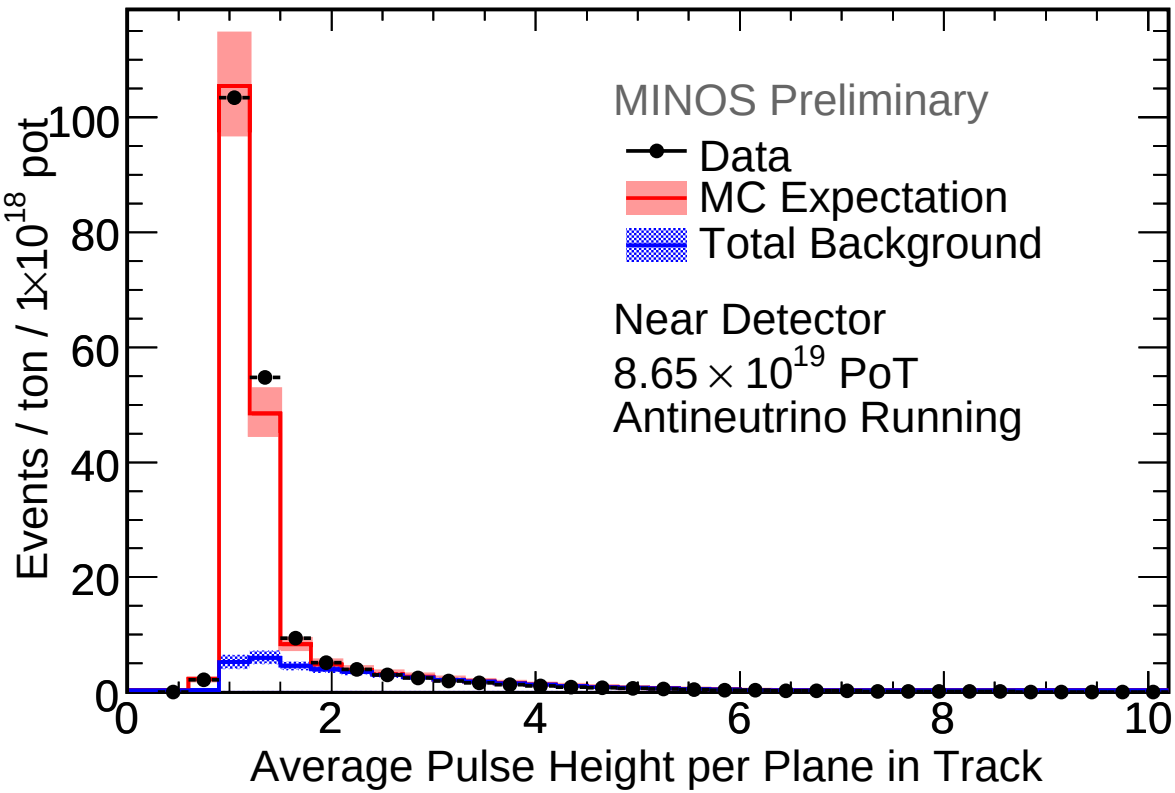

Figure 9: The mean pulse height in the track, an input to the CC/NC separator, shown in the Near Detector before the CC/NC separation cut has been applied. The red histogram represents the Monte Carlo expectation with the systematic error, the blue histogram represents the total (charged and neutral current) background with the background uncertaintiy. Black points represent data.

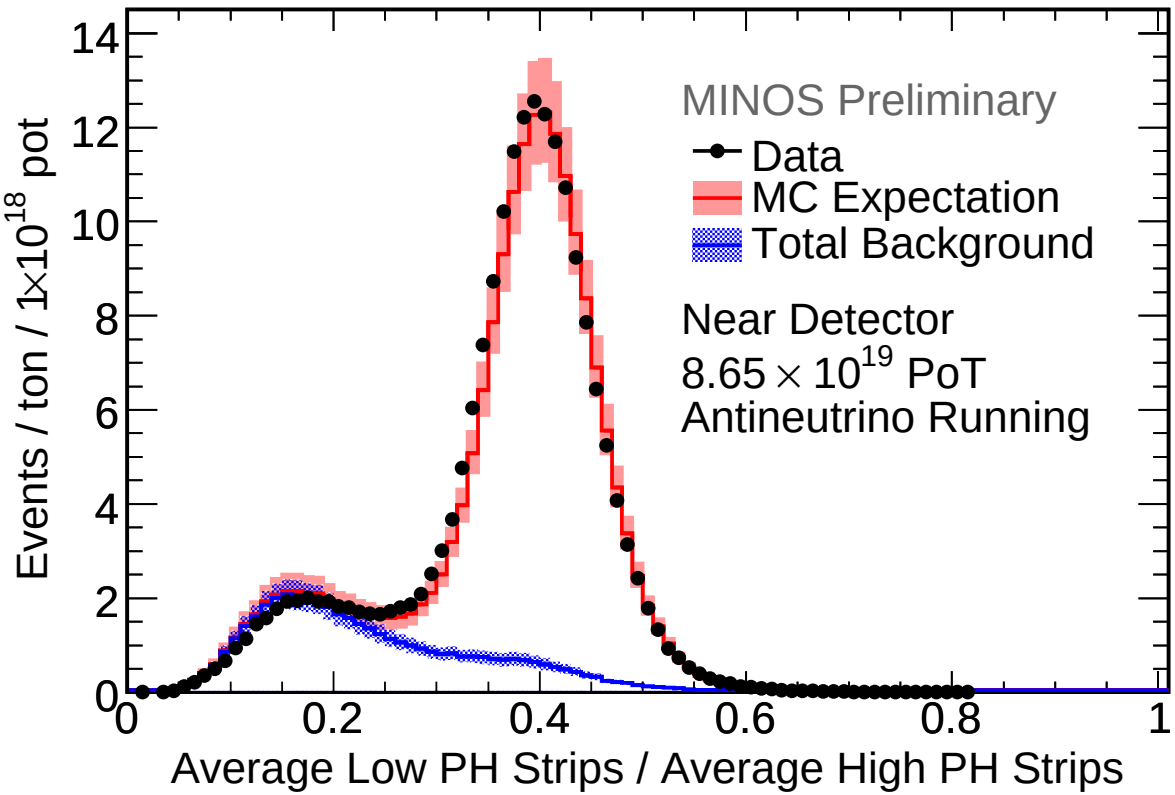

Figure 10: The ratio of mean low pulse height to mean high pulse height, an input to the CC/NC separator, shown in the Near Detector before the CC/NC separation cut has been applied. The red histogram represents the Monte Carlo expectation with the systematic error, the blue histogram represents the total (charged and neutral current) background with the background uncertaintiy. Black points represent data.

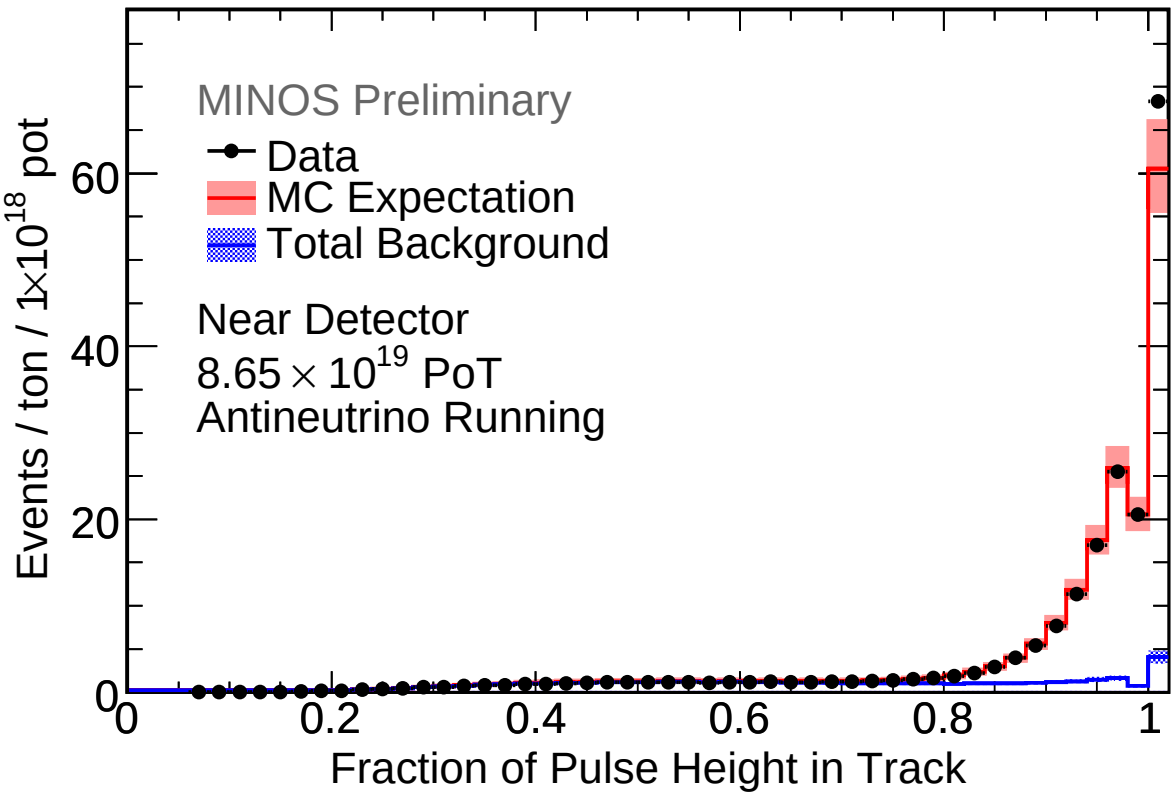

Figure 11: The transverse profile parameter, an input to the CC/NC separator, shown in the Near Detector before the CC/NC separation cut has been applied. The red histogram represents the Monte Carlo expectation with the systematic error, the blue histogram represents the total (charged and neutral current) background with the background uncertaintiy. Black points represent data.

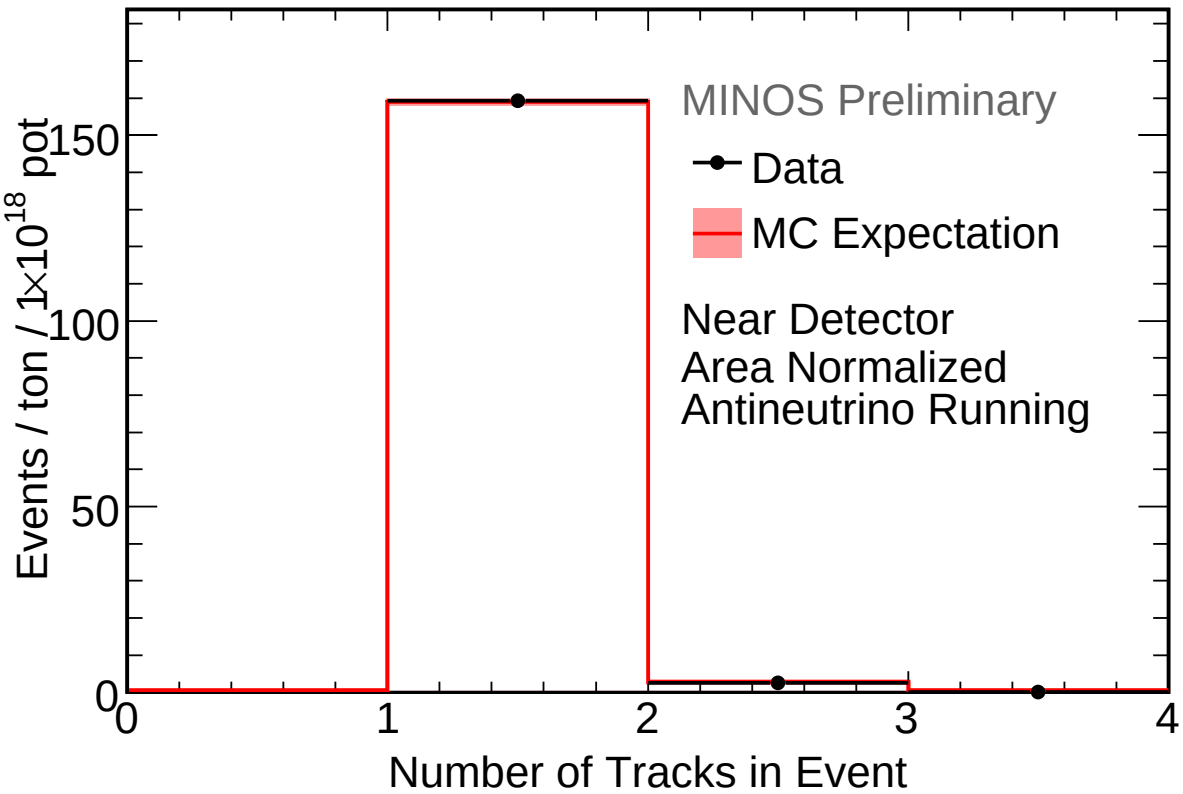

Figure 12: The number of tracks in selected charged current antineutrino interactions in the Near Detector. The red histogram represents the Monte Carlo expectation with the systematic error and black points represent data.

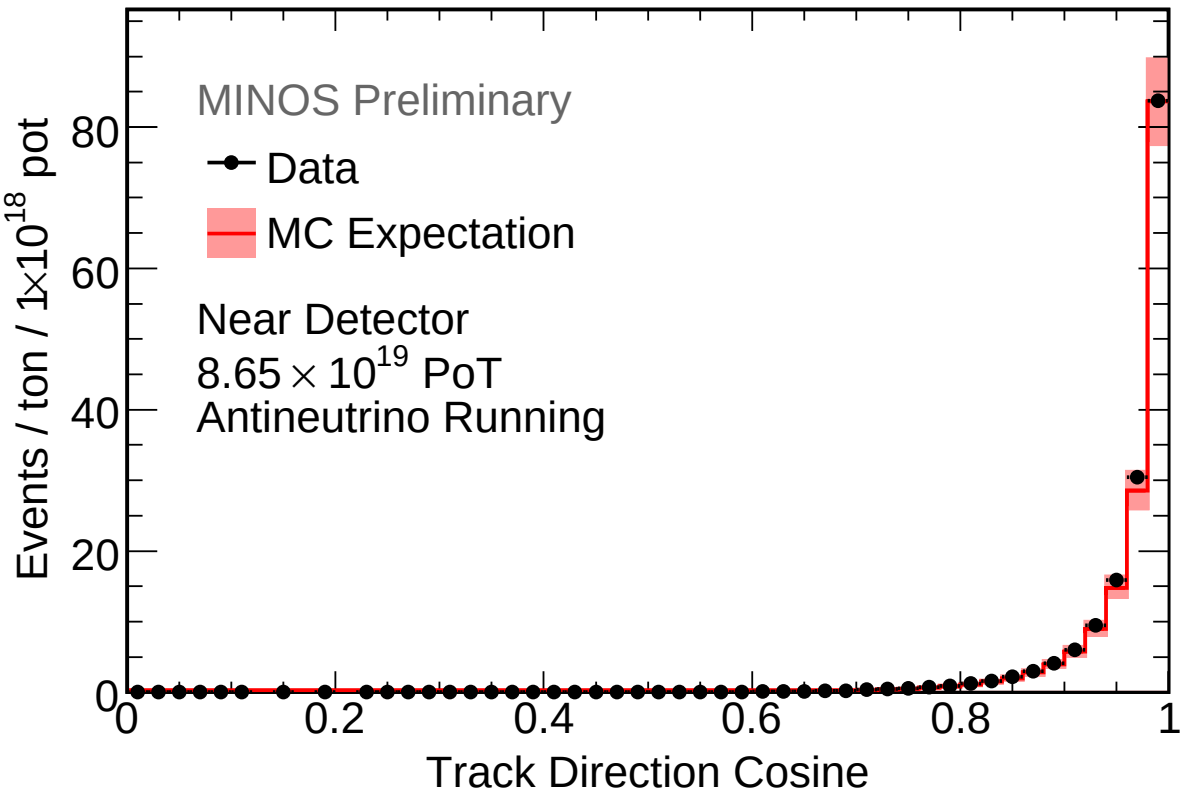

Figure 13: Cosine of the angle between the muon track and beam direction for events selected as antineutrinos in the Near Detector. The red histogram represents the Monte Carlo expectation with the systematic error and black points represent data.

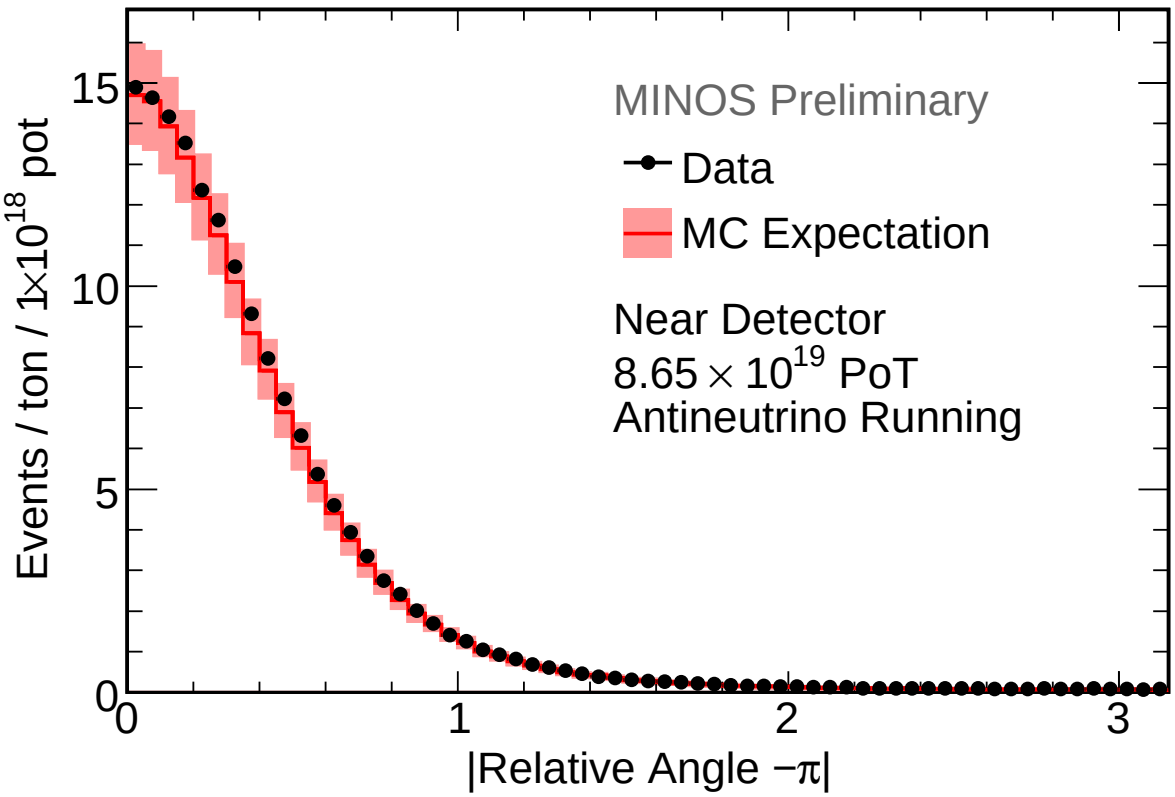

Figure 14: The $|\text{Relative Angle} - \pi$ distribution for events selected as antineutrinos in the Near Detector. The red histogram represents the Monte Carlo expectation with the systematic error and black points represent data.

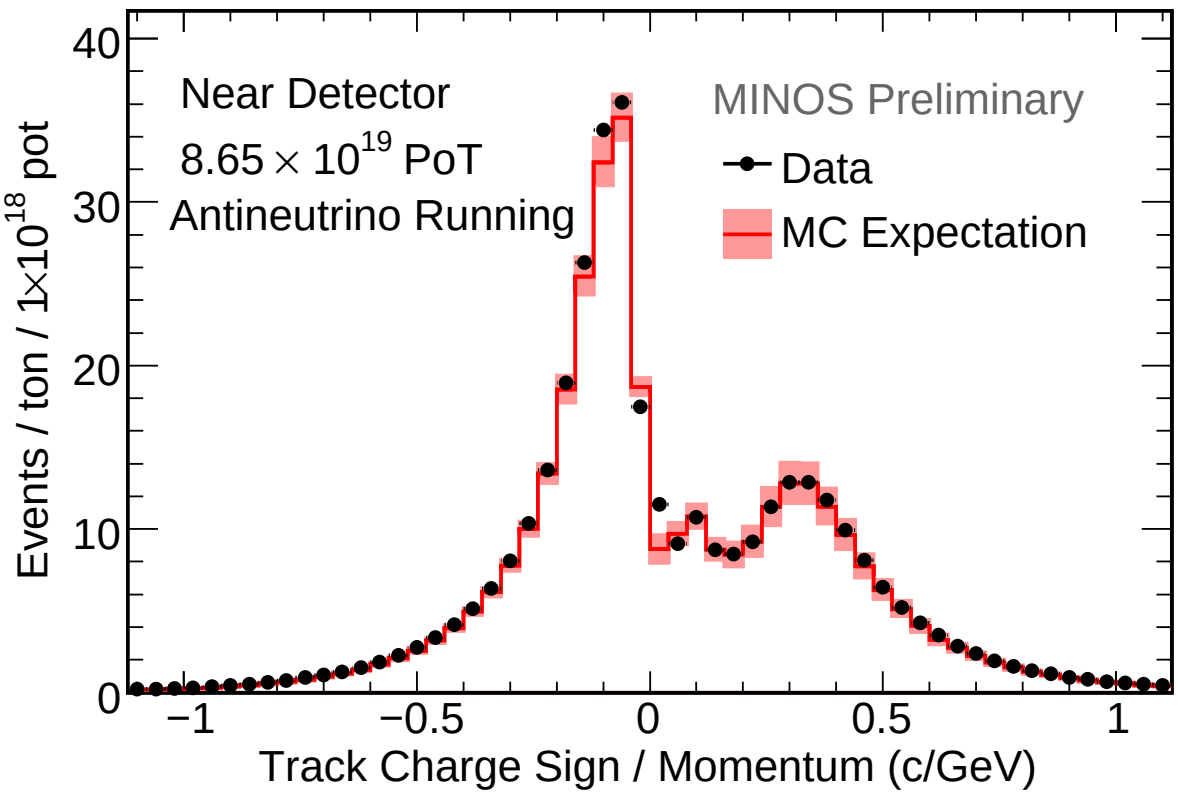

Figure 15: The charge to momentum ratio, (q/p), of selected events before charge sign selection in the Near Detector. The red curve represents MC expectation with the systematic uncertainty and black dots represent data.

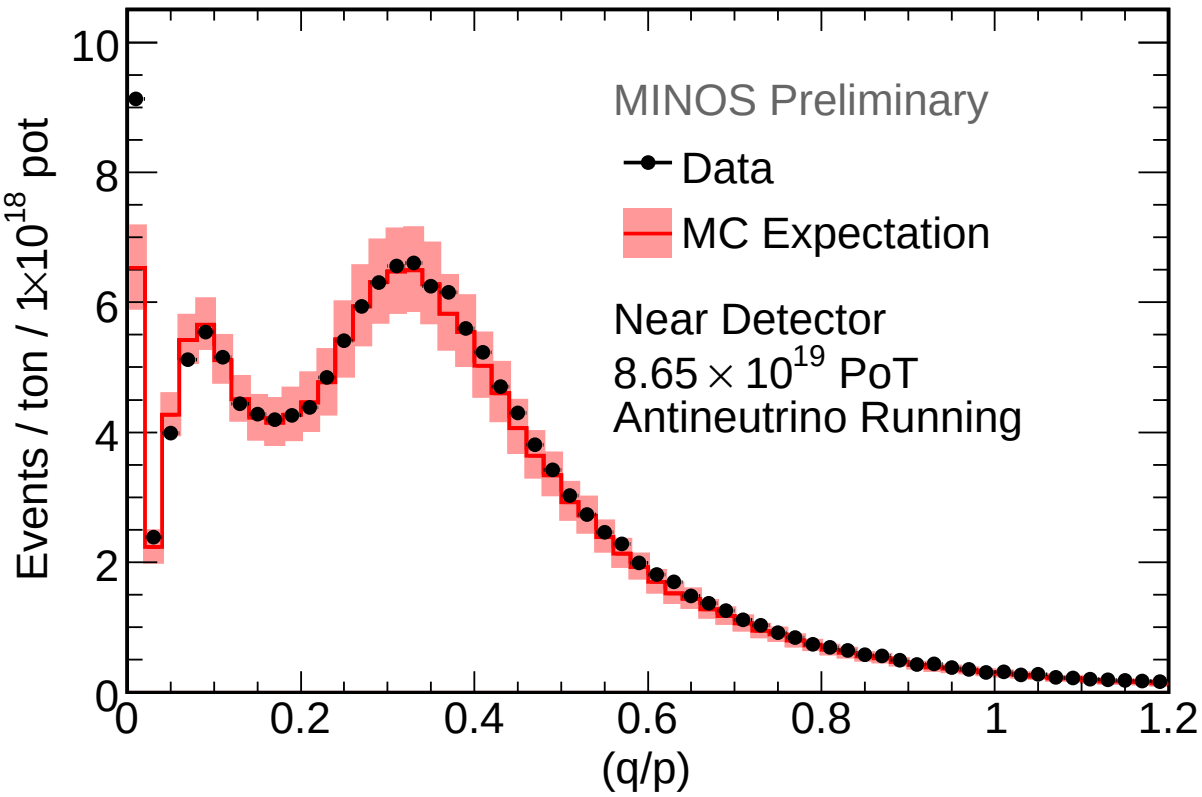

Figure 16: The charge to momentum ratio, (q/p), of selected events in the Near Detector. The red curve represents MC expectation with the systematic uncertainty and black dots represent data.

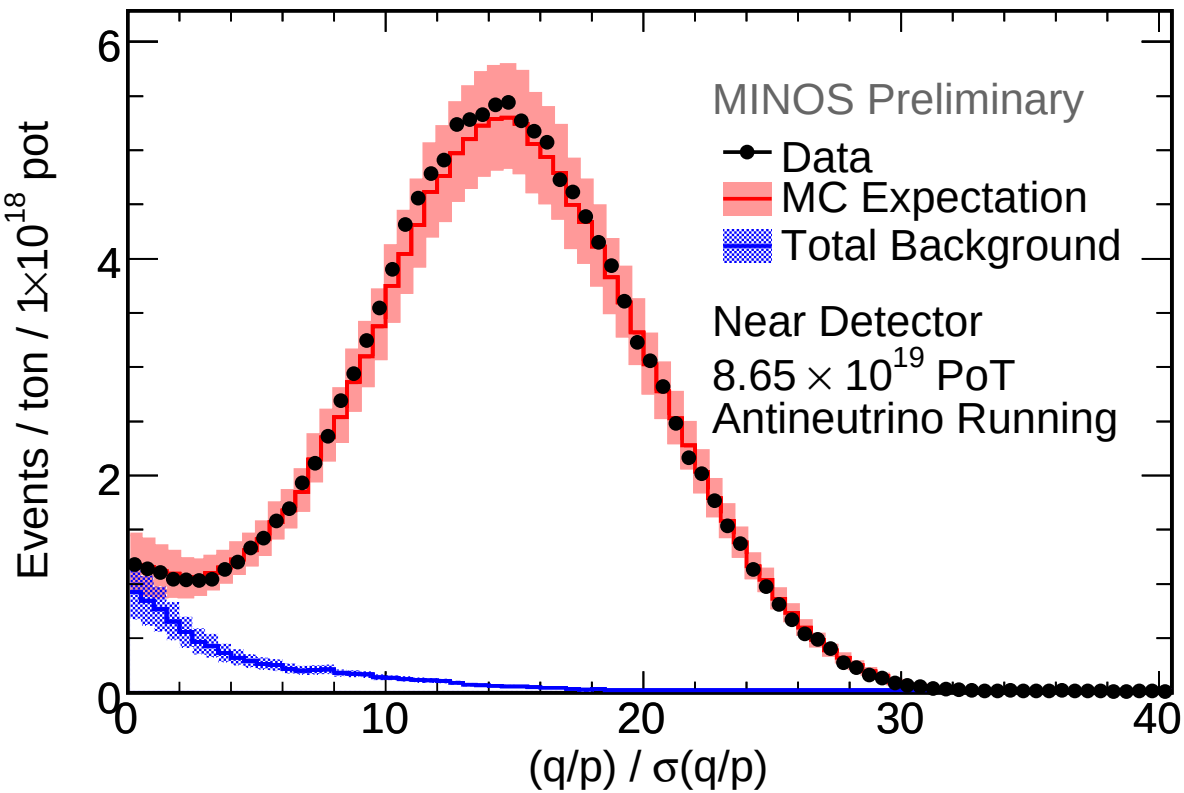

Figure 17: The track charge sign significance, $(q/p)/\sigma(q/p)$, of selected antineutrino events in the Near Detector. The red curve represents MC expectation with the systematic uncertainty, the blue curve represents the CC and NC backgrounds with systematic errors and black dots represent data.

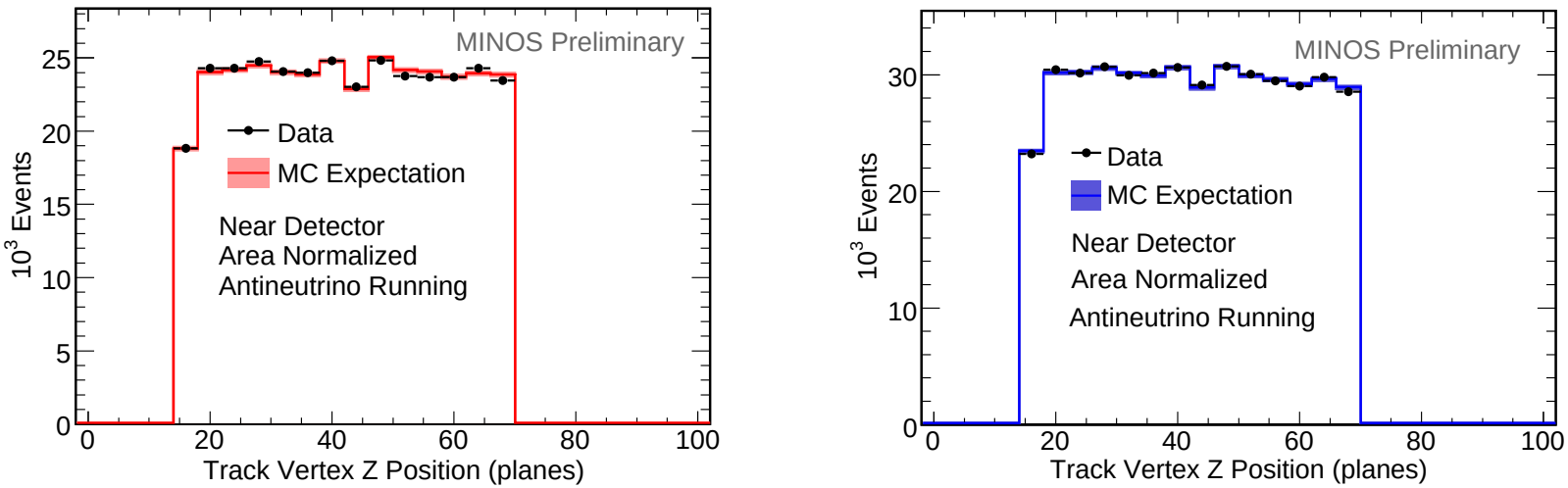

Figure 18: Near Detector track vertex longitudinal position distribution in planes for antineutrinos (red, left) and neutrinos (blue, right). The colored histogram represents the Monte Carlo expectation with the systematic error and black points represent data.

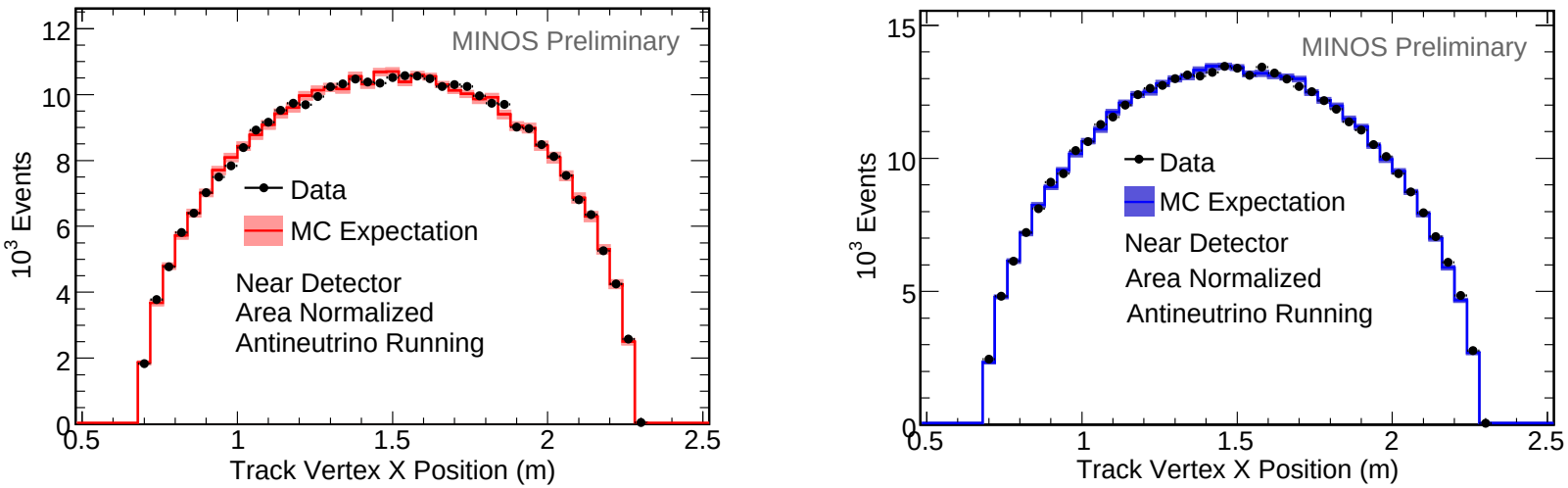

Figure 19: Near Detector track vertex X position distribution for antineutrinos (red, left) and neutrinos (blue, right). The colored histogram represents the Monte Carlo expectation with the systematic error and black points represent data.

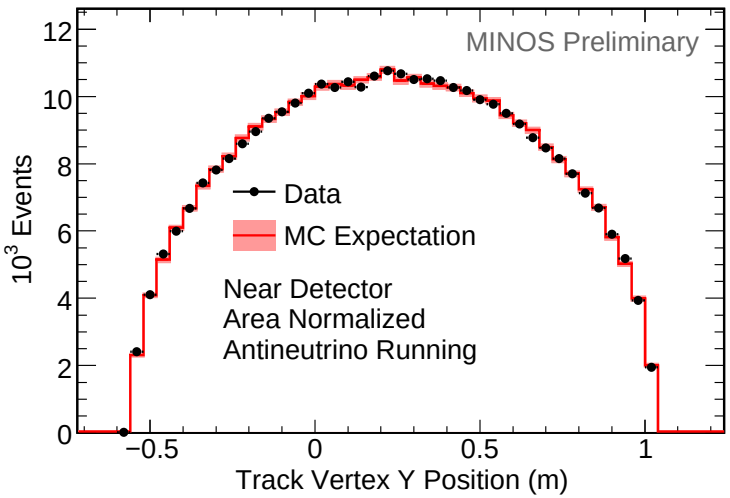

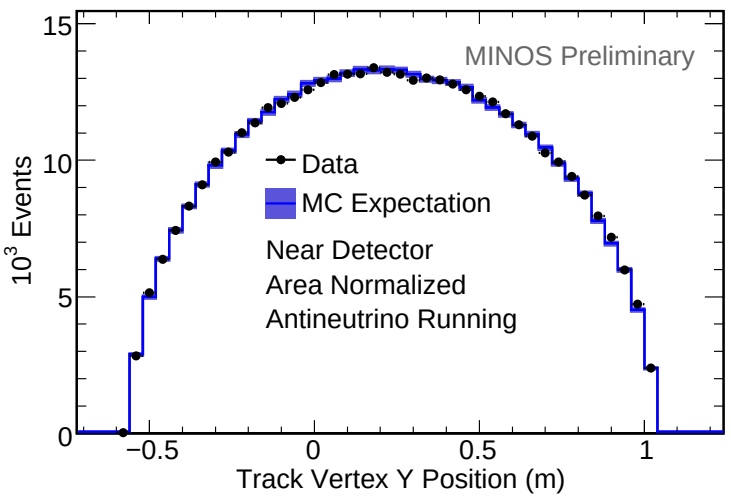

Figure 20: Near Detector track vertex Y position distribution for antineutrinos (red, left) and neutrinos (blue, right). The colored histogram represents the Monte Carlo expectation with the systematic error and black points represent data.

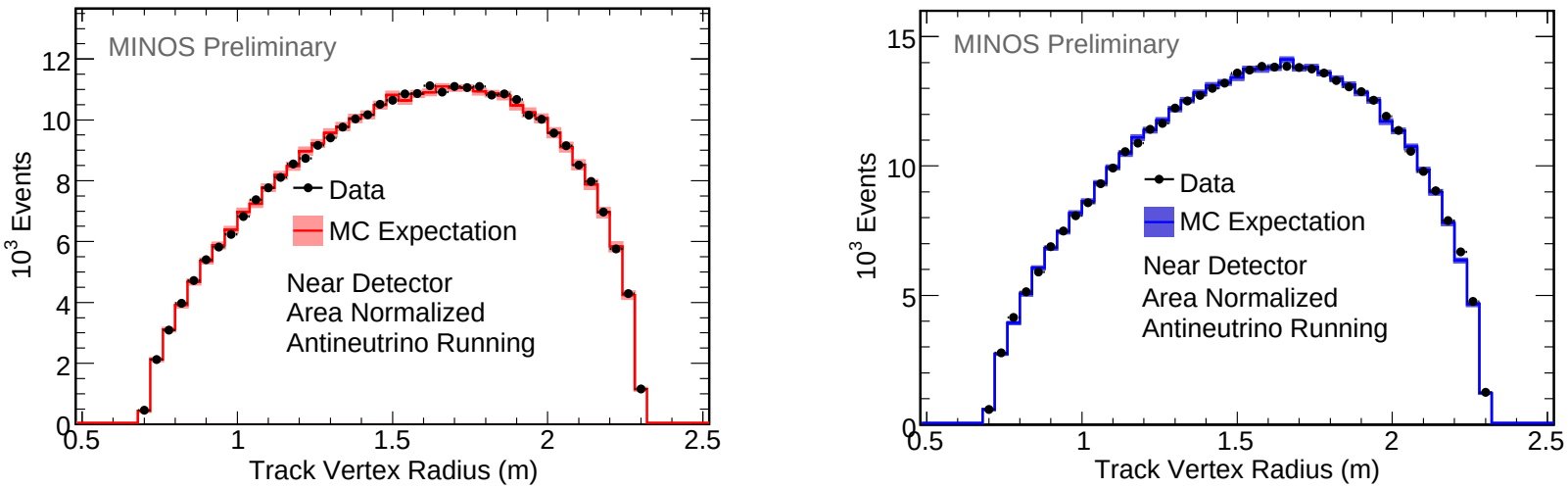

Figure 21: Near Detector track vertex radius distribution for antineutrinos (red, left) and neutrinos (blue, right). The colored histogram represents the Monte Carlo expectation with the systematic error and black points represent data.

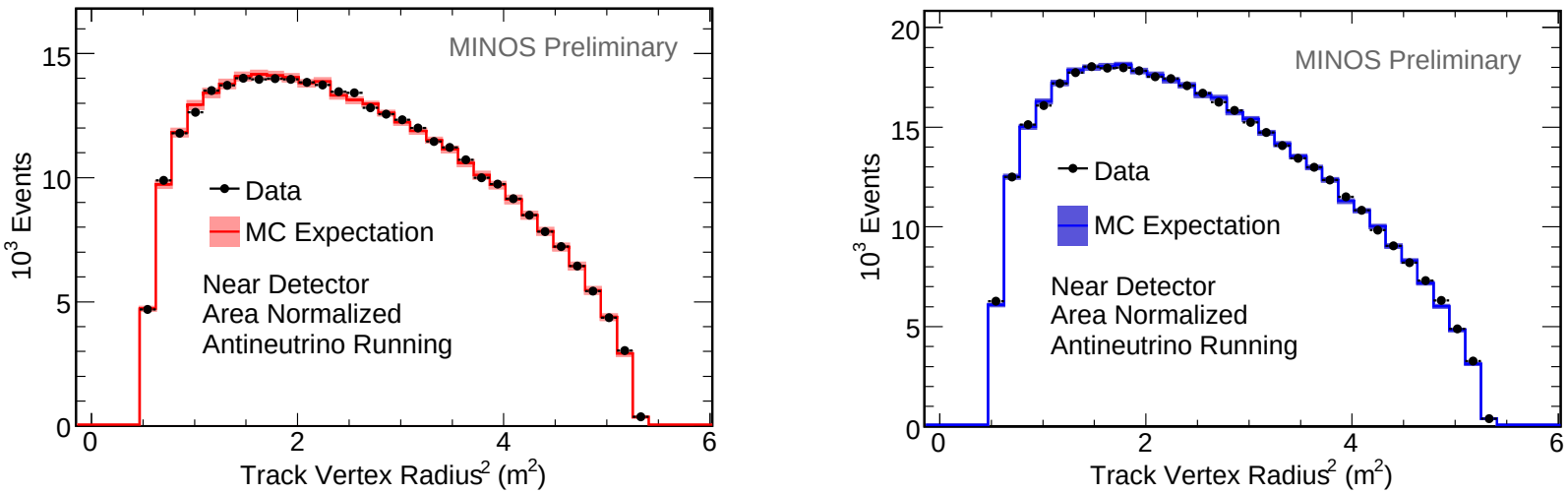

Figure 22: Near Detector track vertex radius^2 distribution for antineutrinos (red, left) and neutrinos (blue, right). The colored histogram represents the Monte Carlo expectation with the systematic error and black points represent data.

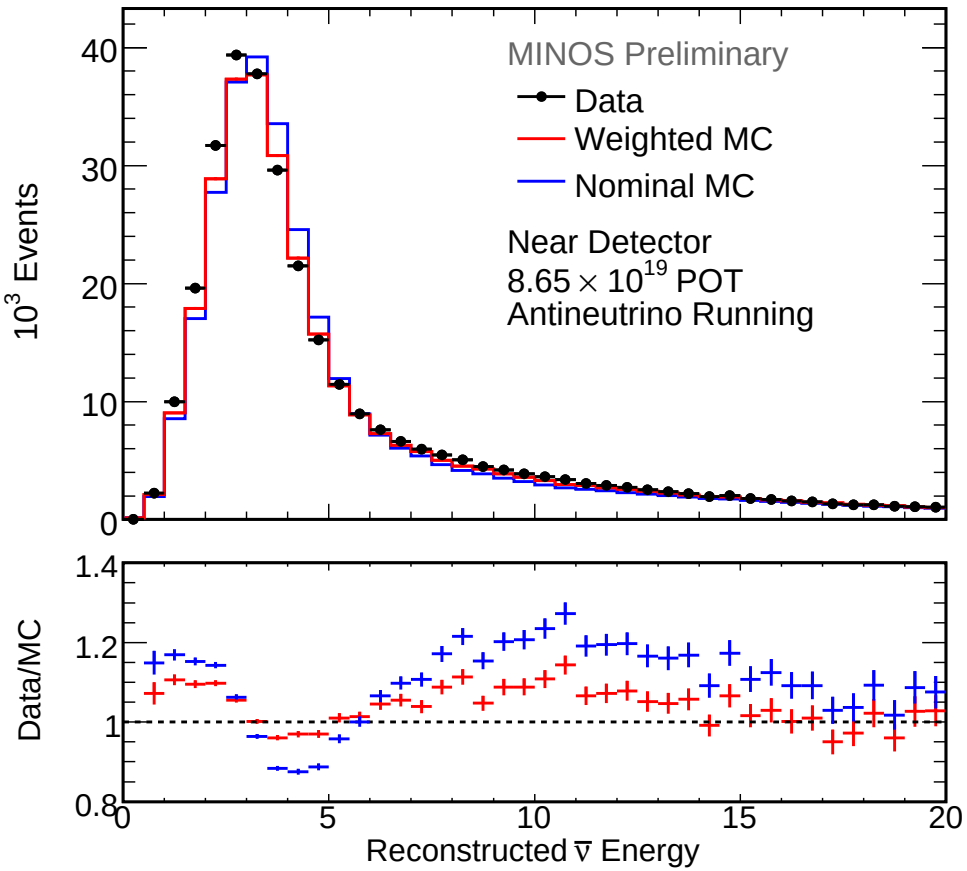

Figure 23: The reconstructed energy distribution of selected antineutrinos in the near detector. The black points represent data, the blue line represents nominal (untuned) Monte Carlo and the red line represents the Monte Carlo with a tuned flux (SKZP weighted).

ND Data Stability

minos-doc-7210

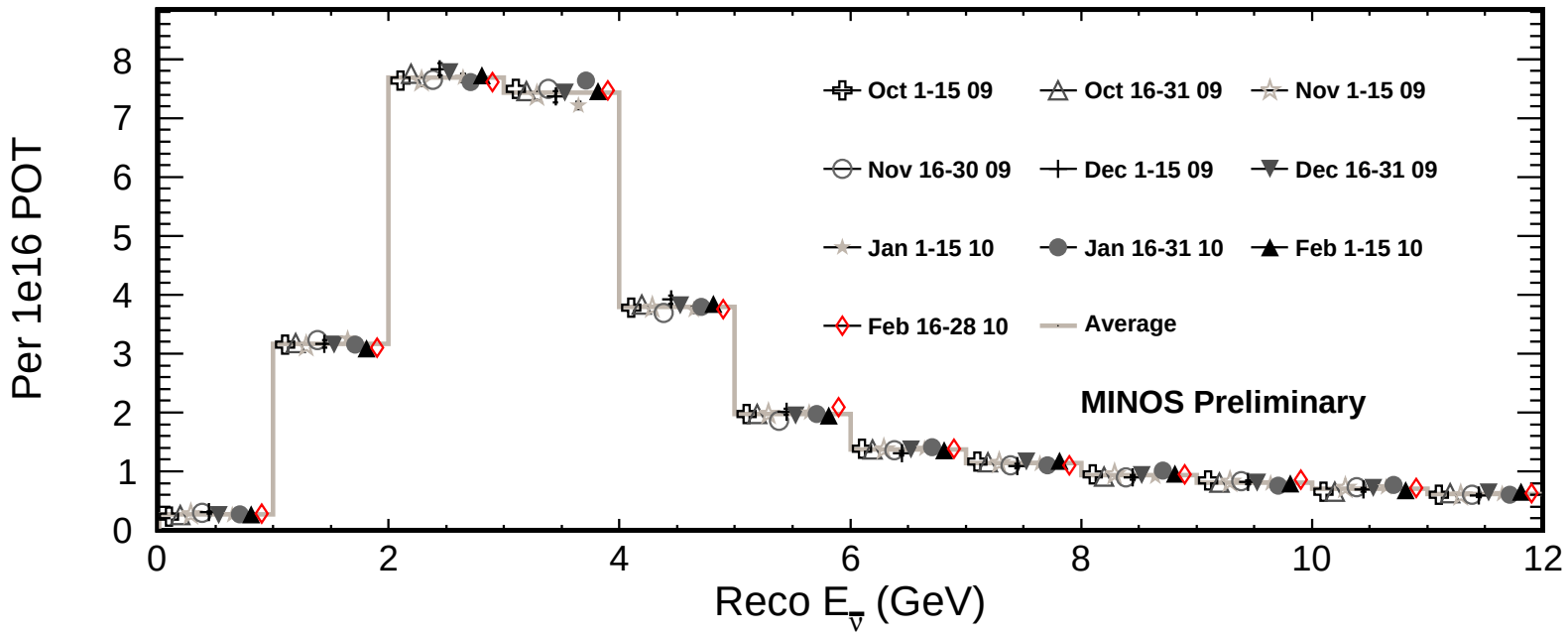

Figure 24: Energy Spectrum in Run IV broken up into time periods. Each individual time period is shown for bins of 1 GeV (normalized to POT). The average number of events in each bin is also shown. Visual inspection shows that for each bin the beam was stable during Run IV. minos-doc-7210

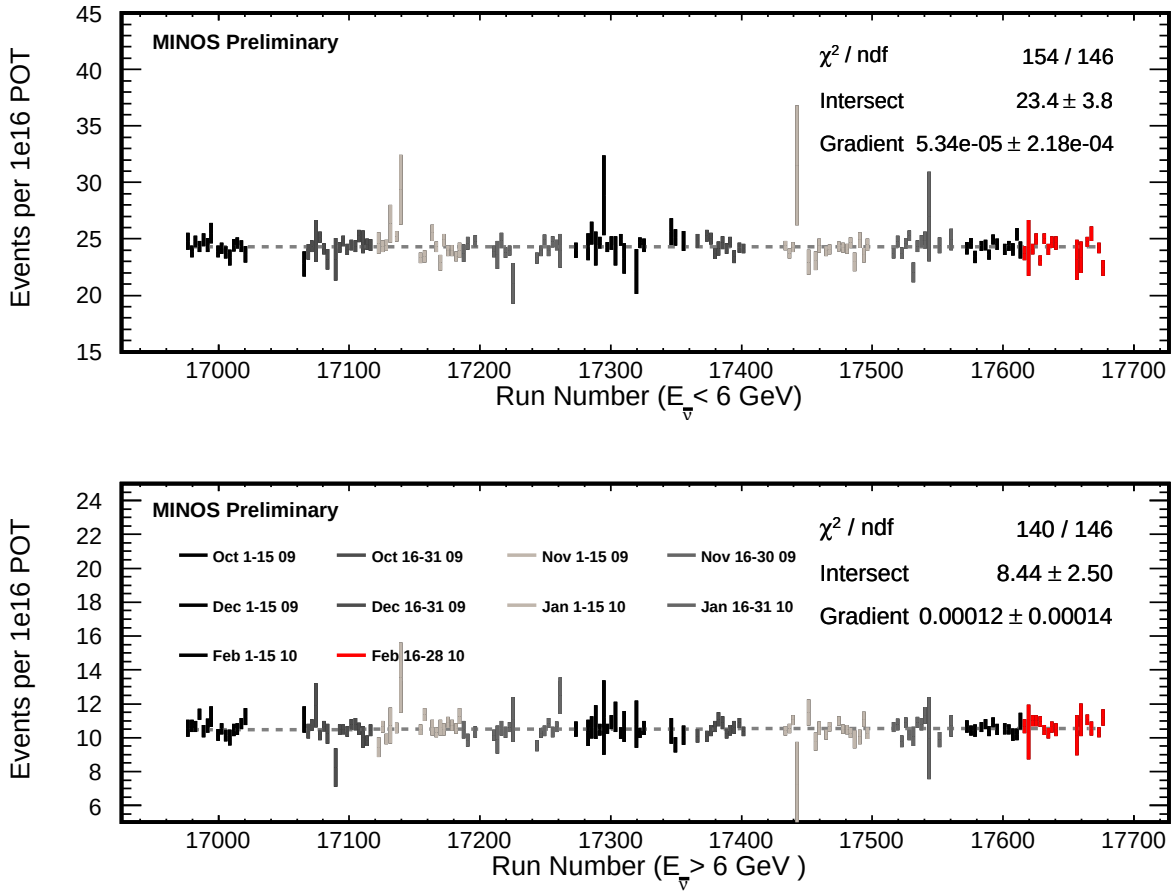

Figure 25: The event rate vs. run number during Run IV, divided into two parts: events in the beam peak (above) and events in the high energy tail (below). Each data set was then fit to a line separately. The results of the fits are shown from which we can conclude that the beam was stable through out Run IV. minos-doc-7210

FD Data/MC distributions

minos-doc-7340

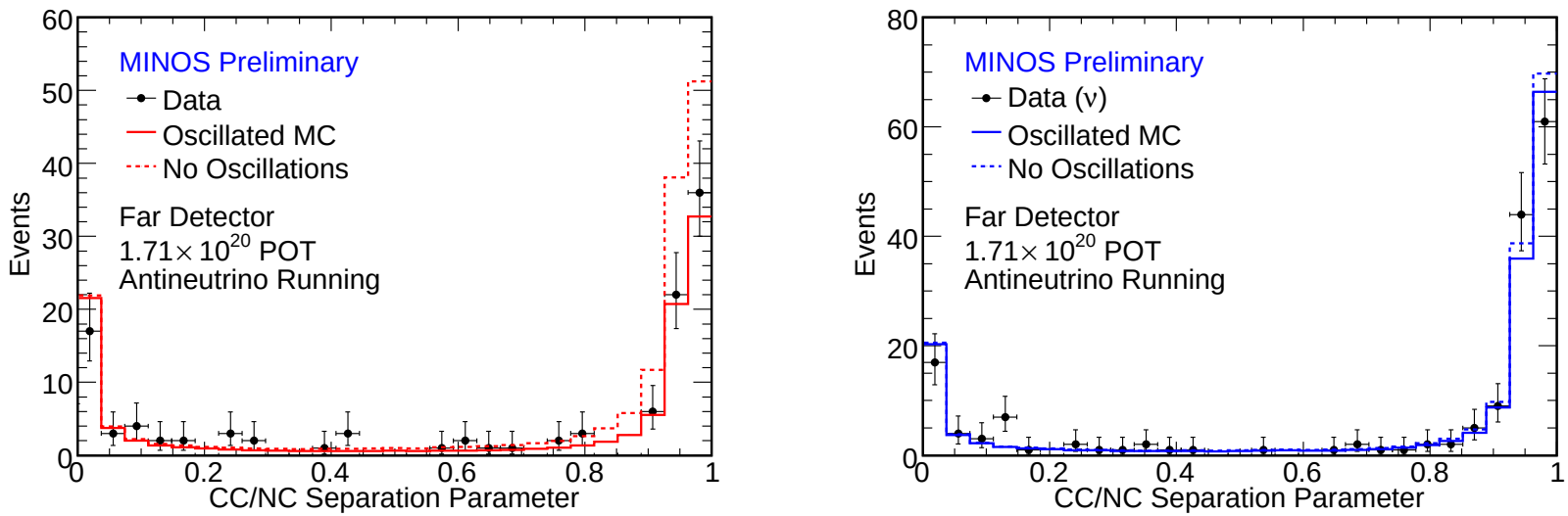

Figure 26: Distribution of the CC/NC separation parameter for $\overline{\nu}_\mu$ events (left, red) and ν_μ events (right, blue) in the Far Detector before the CC/NC separation cut has been applied. The solid colored histograms represents the Monte Carlo expectation with the best fit oscillation parameters, the dashed colored histograms represents the no oscillations expectation and black points represent data. MC is pot normalized to data.

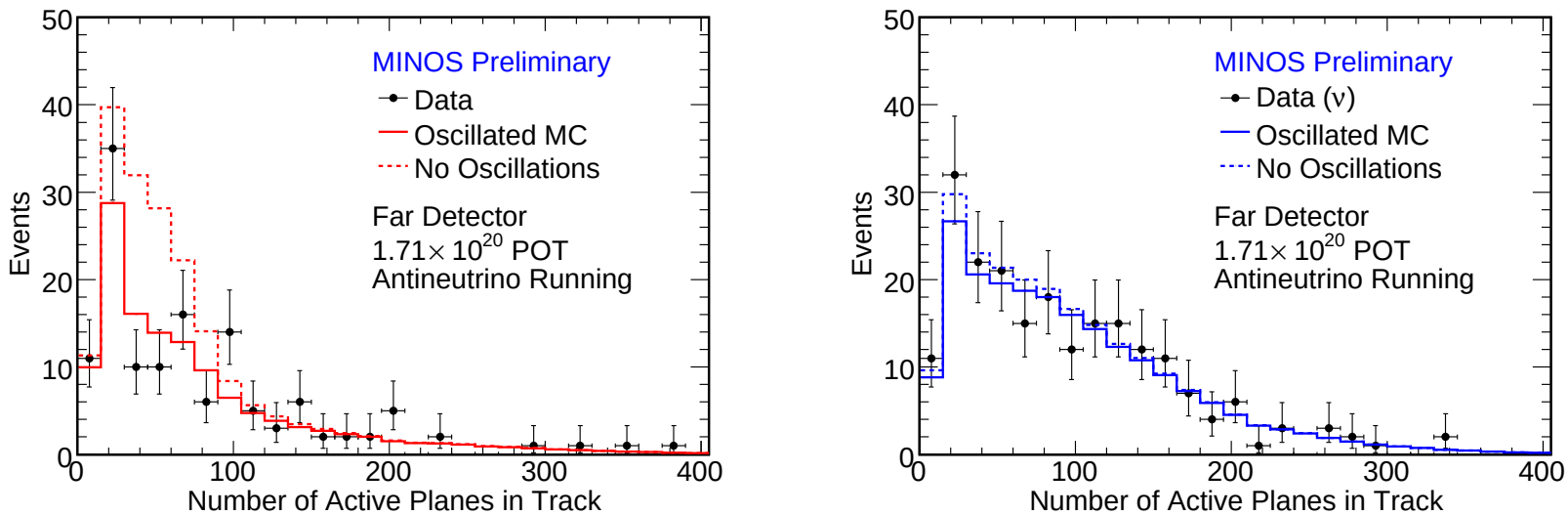

Figure 27: The number of active scintillator planes in the track, an input to the CC/NC separator, in the Far Detector for $\overline{\nu}_\mu$ events (left, red) and ν_μ events (right, blue) before the CC/NCC separation cut has been applied. The red histogram represents the Monte Carlo expectation with current best fit oscillation parameters, the dashed red histogram represents the no oscillations case. Black points represent data.

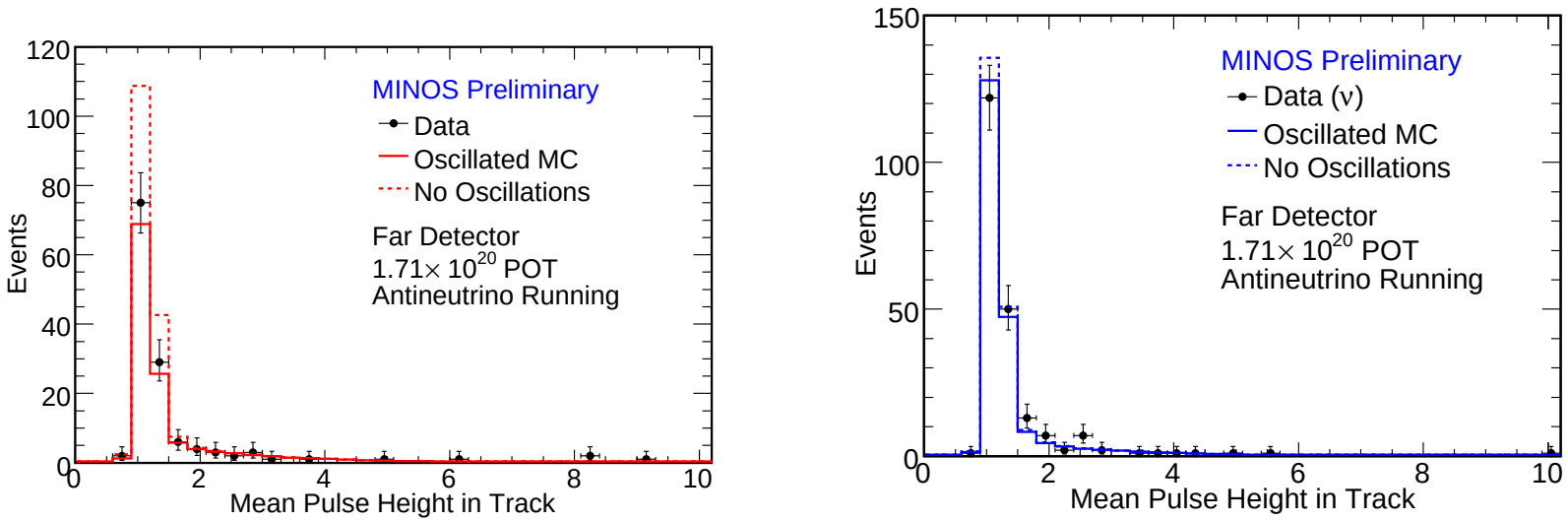

Figure 28: The mean pulse height in the track, an input to the CC/NC separator, in the Far Detector for $\overline{\nu}_\mu$ events (left, red) and ν_μ events (right, blue) before the CC/NCC separation cut has been applied. The red histogram represents the Monte Carlo expectation with current best fit oscillation parameters, the dashed red histogram represents the no oscillations case. Black points represent data.

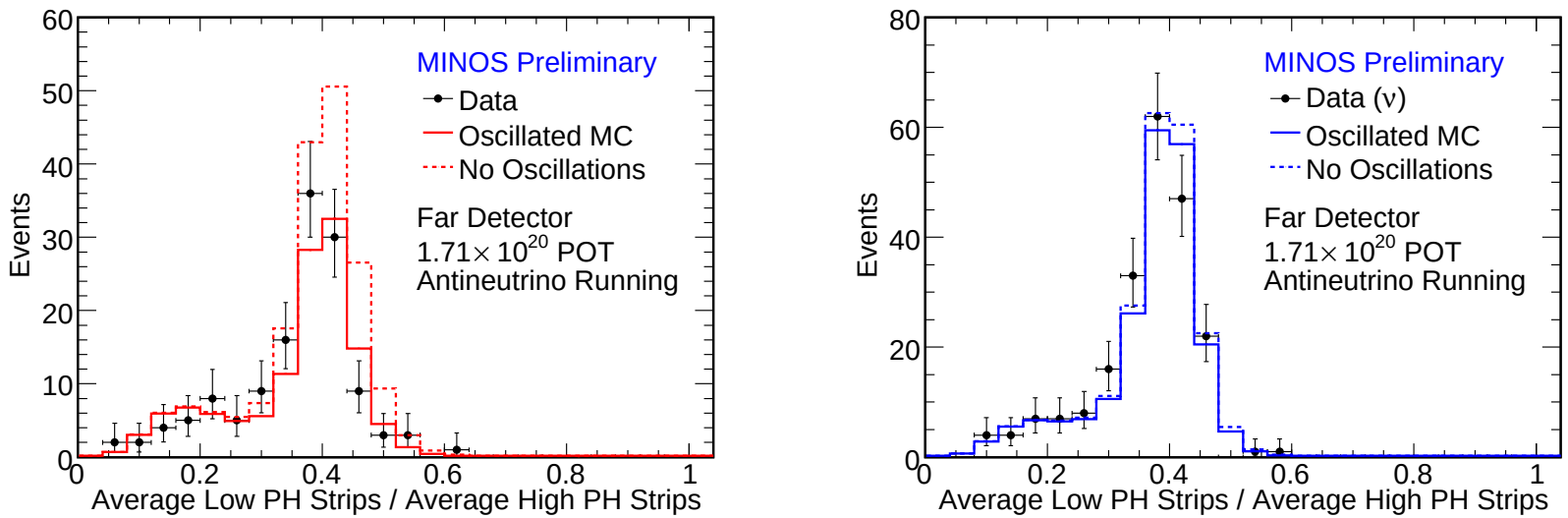

Figure 29: The ratio of mean low pulse height to mean high pulse height in track hits, an input to the CC/NC separator, in the Far Detector for $\overline{\nu}_\mu$ events (left, red) and ν_μ events (right, blue) before the CC/NCC separation cut has been applied. The red histogram represents the Monte Carlo expectation with current best fit oscillation parameters, the dashed red histogram represents the no oscillations case. Black points represent data.

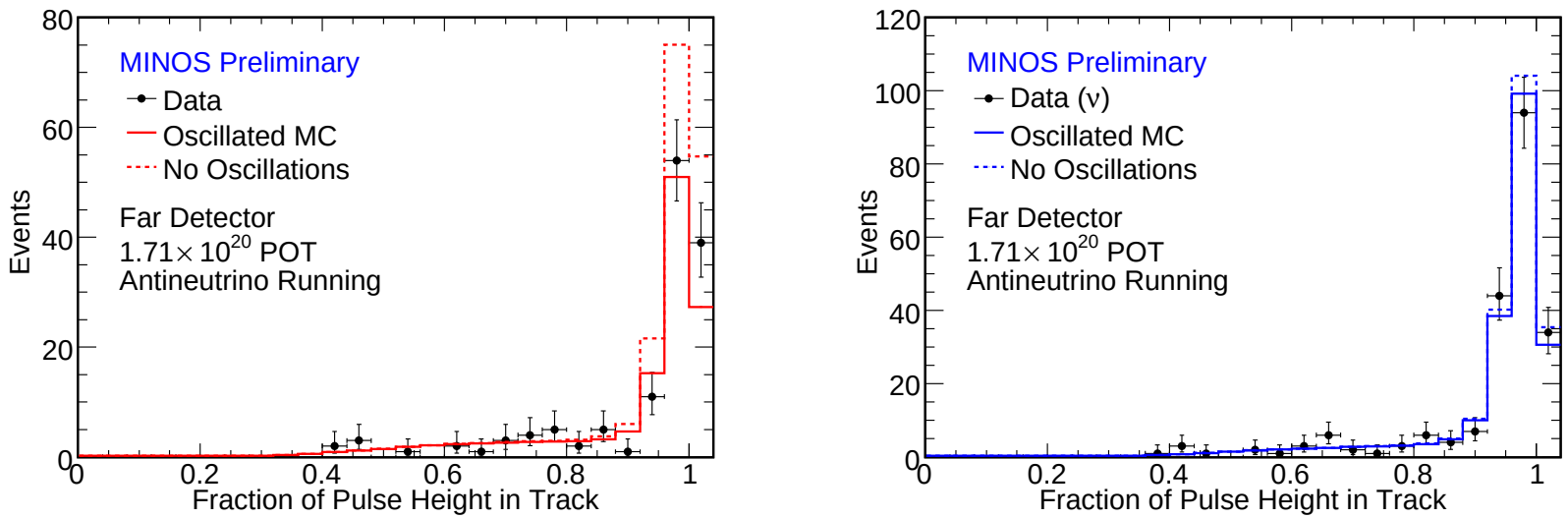

Figure 30: The transverse profile parameter, an input to the CC/NC separator which measures the fraction of pulse height in the muon track, in the Far Detector for $\overline{\nu}_\mu$ events (left, red) and ν_μ events (right, blue) before the CC/NCC separation cut has been applied. The red histogram represents the Monte Carlo expectation with current best fit oscillation parameters, the dashed red histogram represents the no oscillations case. Black points represent data.

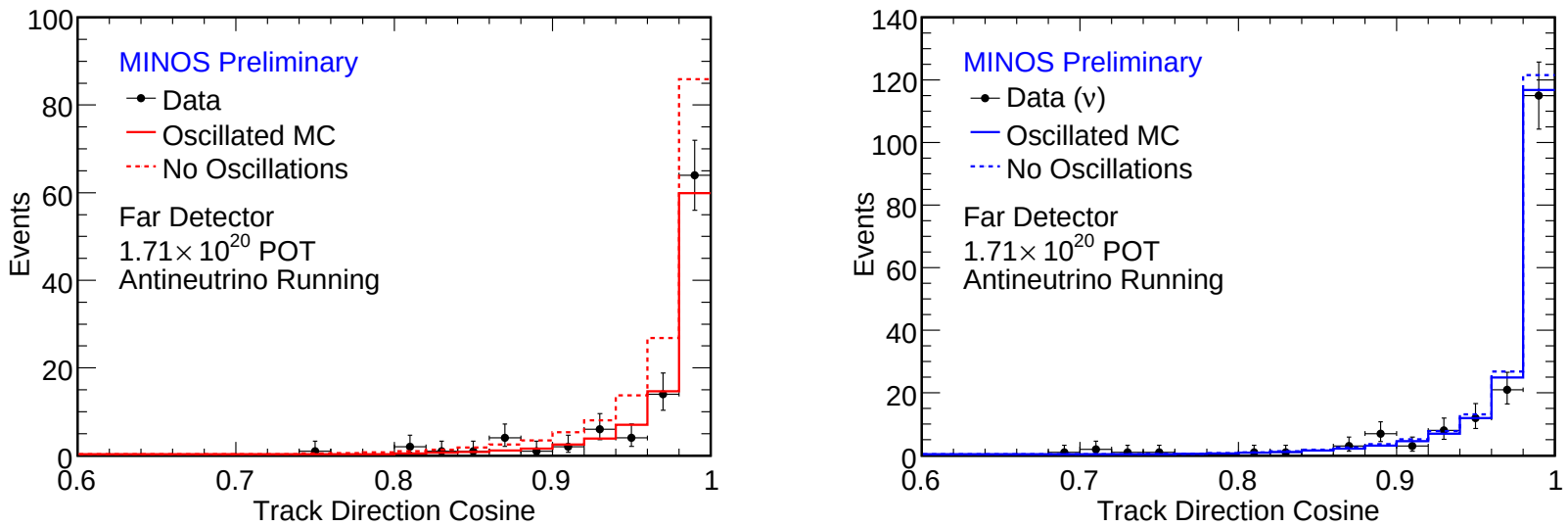

Figure 31: Cosine of the angle between the muon track and beam direction of selected $\overline{\nu}_\mu$ events (left, red) and ν_μ events (right, blue) in the Far Detector. The solid colored histograms represents the Monte Carlo expectation with the best fit oscillation parameters, the dashed colored histograms represents the no oscillations expectation and black points represent data. MC is pot normalized to data. Preselection removes events with $\theta < 0.6$ to reduce background from cosmic rays.

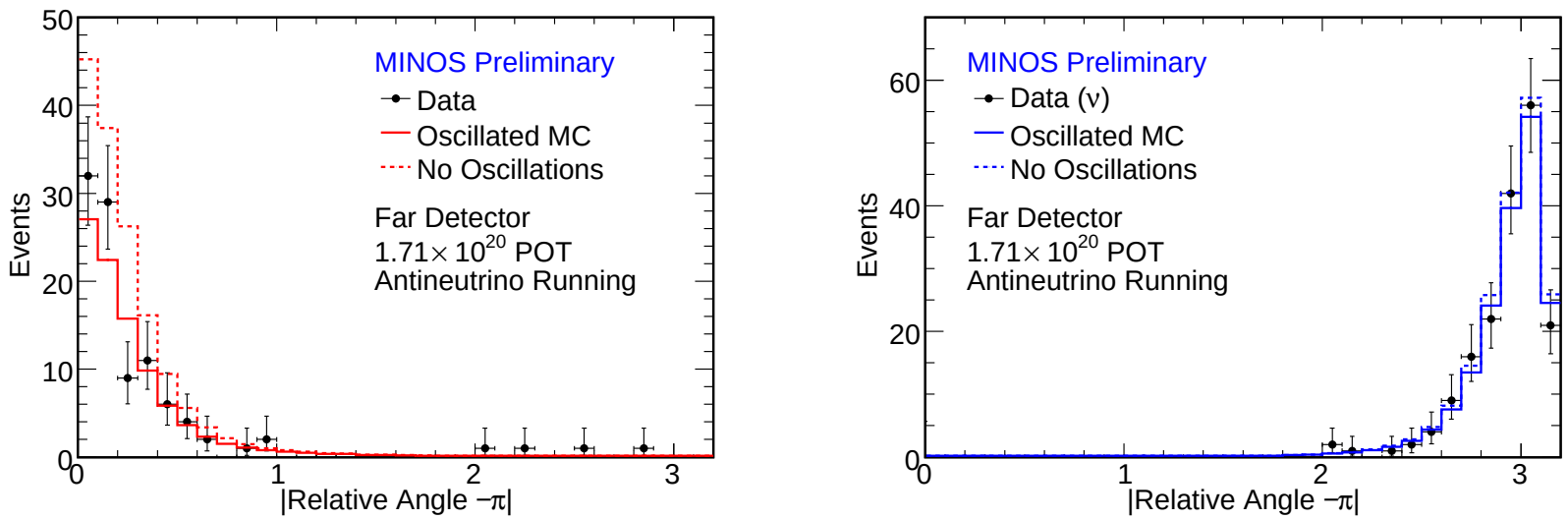

Figure 32: $|\mathrm{RelativeAngle} - \pi|$ distribution of selected $\overline{\nu}_\mu$ events (left, red) and ν_μ events (right, blue) in the Far Detector. The solid colored histograms represents the Monte Carlo expectation with the best fit oscillation parameters, the dashed colored histograms represents the no oscillations expectation and black points represent data. MC is pot normalized to data.

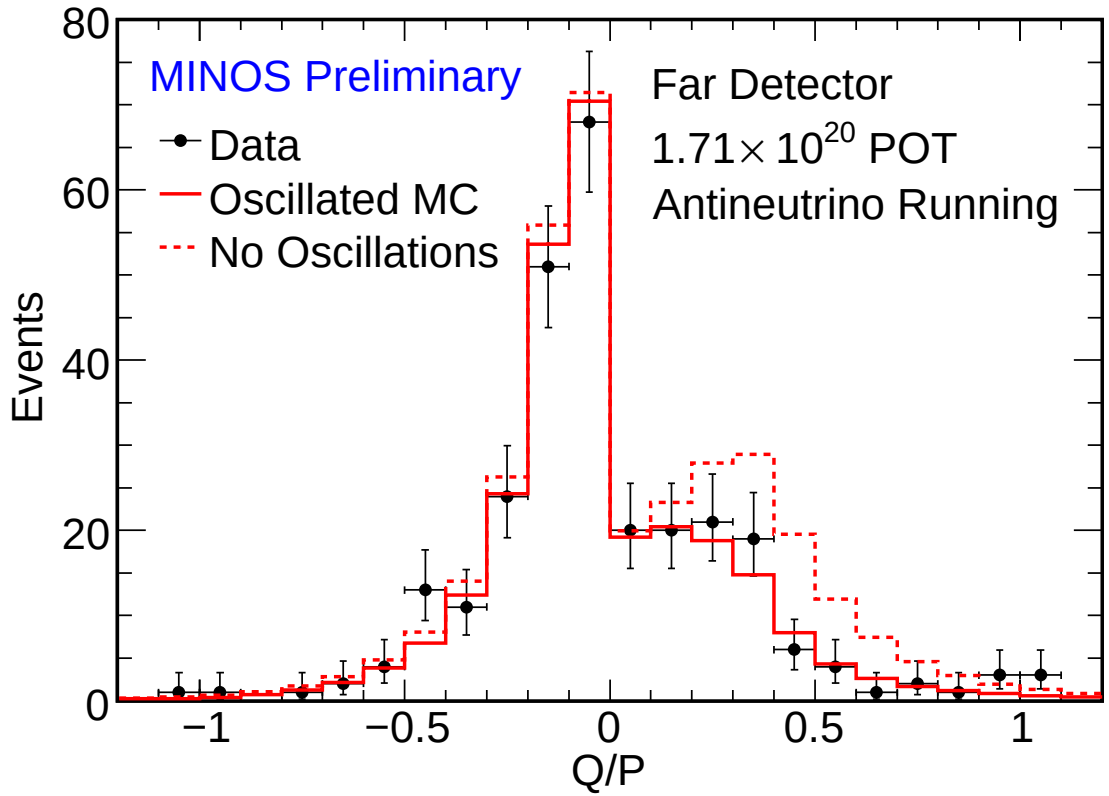

Figure 33: The charge-to-momentum ratio, (q/p), of selected Far Detector events before charge sign selection. The solid red curve represents MC with oscillations, the dashed red curve represents no oscillations MC and the black points represent data.

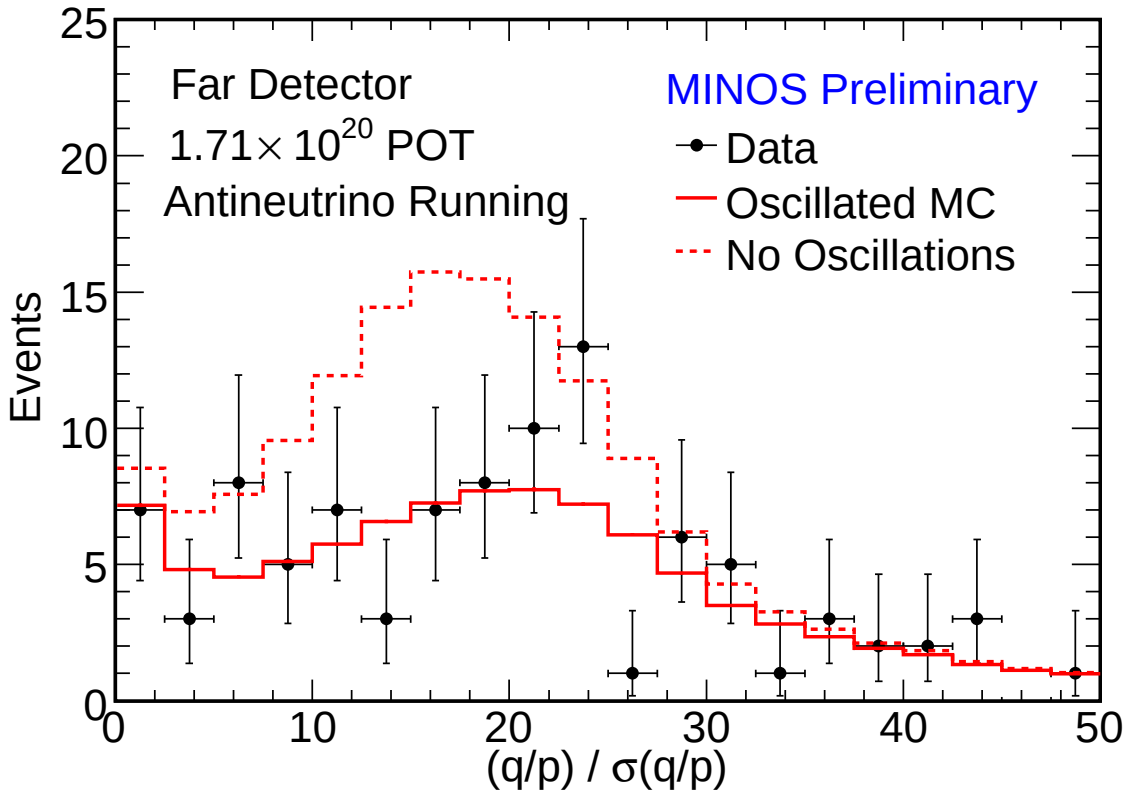

Figure 34: The track charge sign significance, $(q/p)/\sigma(q/p)$, of selected Far Detector $\overline{\nu}_\mu$ events. The solid red curve represents MC with oscillations, the dashed red curve represents no oscillations MC and the black points represent data.

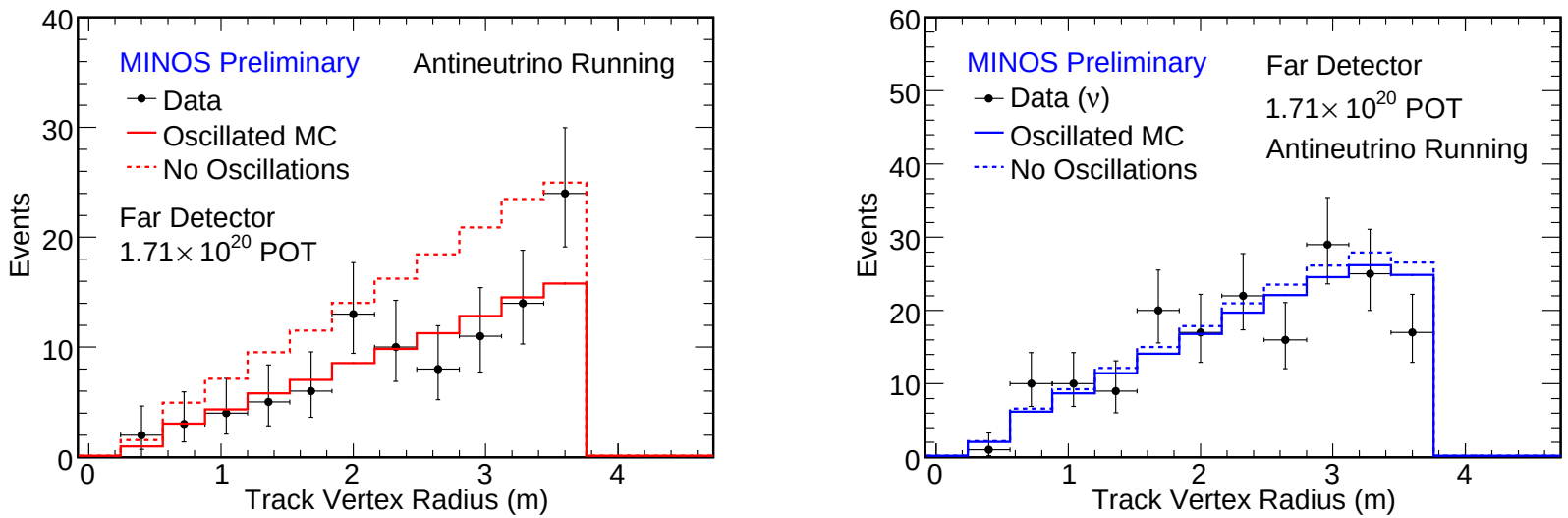

Figure 35: Track vertex radius distribution of selected $\overline{\nu}_\mu$ events (left, red) and ν_μ events (right, blue) in the Far Detector. The solid colored histograms represents the Monte Carlo expectation with the best fit oscillation parameters, the dashed colored histograms represents the no oscillations expectation and black points represent data. MC is pot normalized to data.

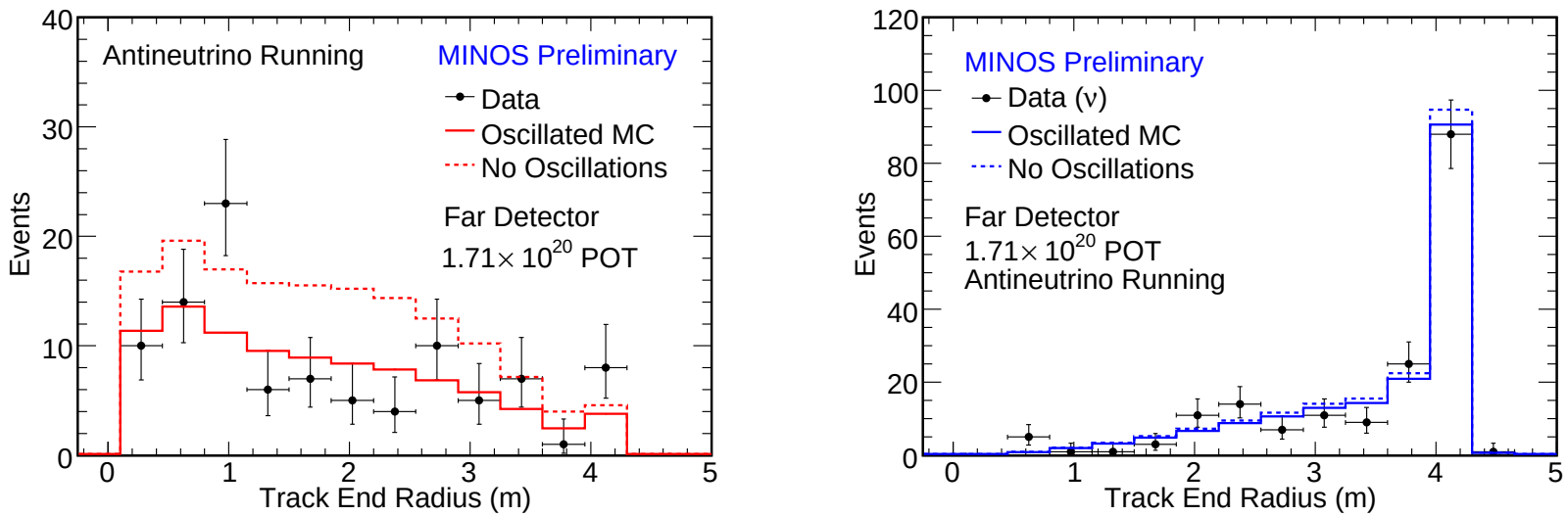

Figure 36: Track end radius distribution of selected $\overline{\nu}_\mu$ events (left, red) and ν_μ events (right, blue) in the Far Detector. The solid colored histograms represents the Monte Carlo expectation with the best fit oscillation parameters, the dashed colored histograms represents the no oscillations expectation and black points represent data. MC is pot normalized to data.

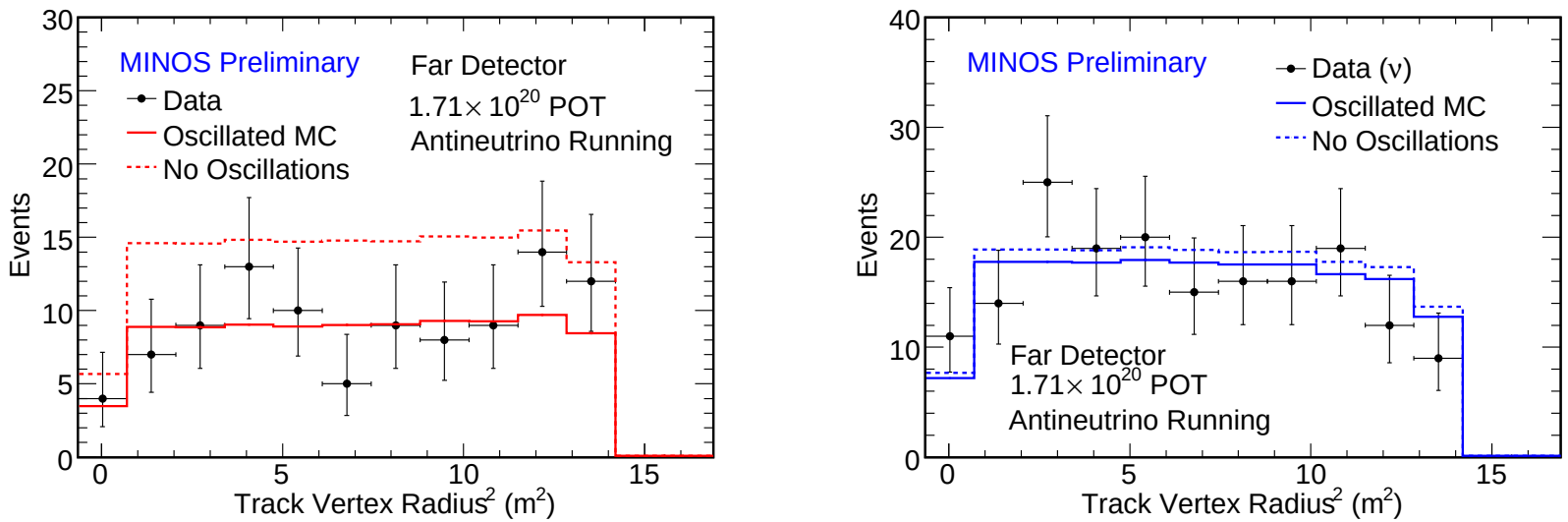

Figure 37: Track vertex radius^2 distribution of selected $\overline{\nu}_\mu$ events (left, red) and ν_μ events (right, blue) in the Far Detector. The solid colored histograms represents the Monte Carlo expectation with the best fit oscillation parameters, the dashed colored histograms represents the no oscillations expectation and black points represent data. MC is pot normalized to data.

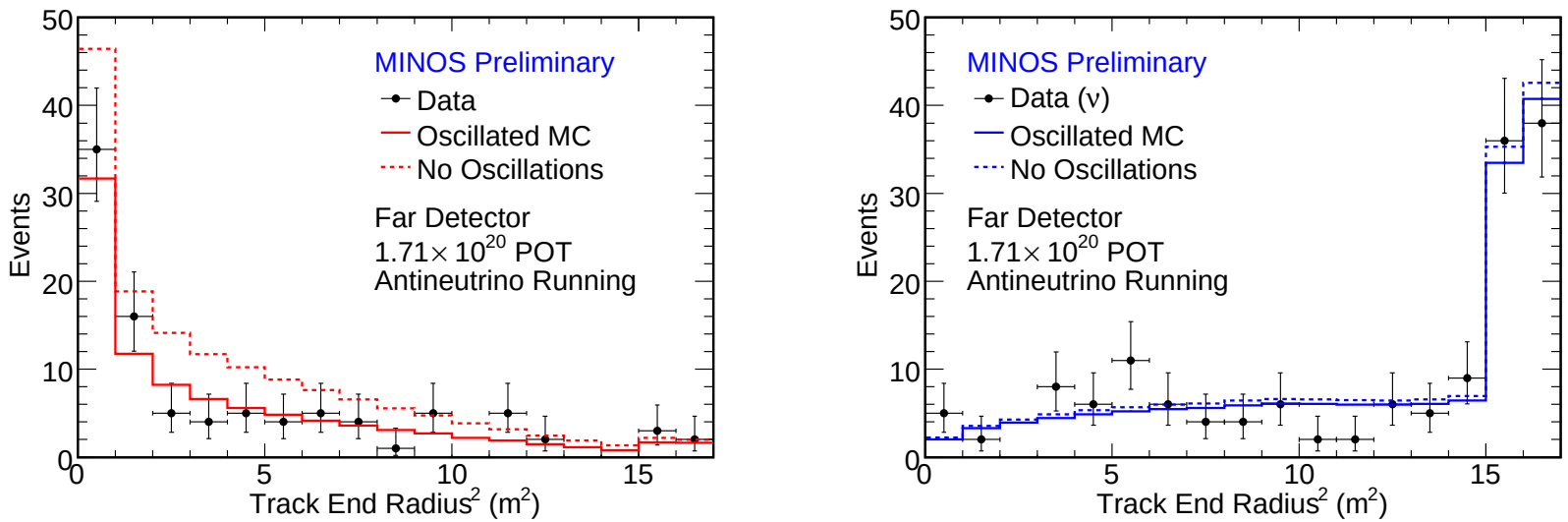

Figure 38: Track end radius^2 distribution of selected $\overline{\nu}_\mu$ events (left, red) and ν_μ events (right, blue) in the Far Detector. The solid colored histograms represents the Monte Carlo expectation with the best fit oscillation parameters, the dashed colored histograms represents the no oscillations expectation and black points represent data. MC is pot normalized to data.

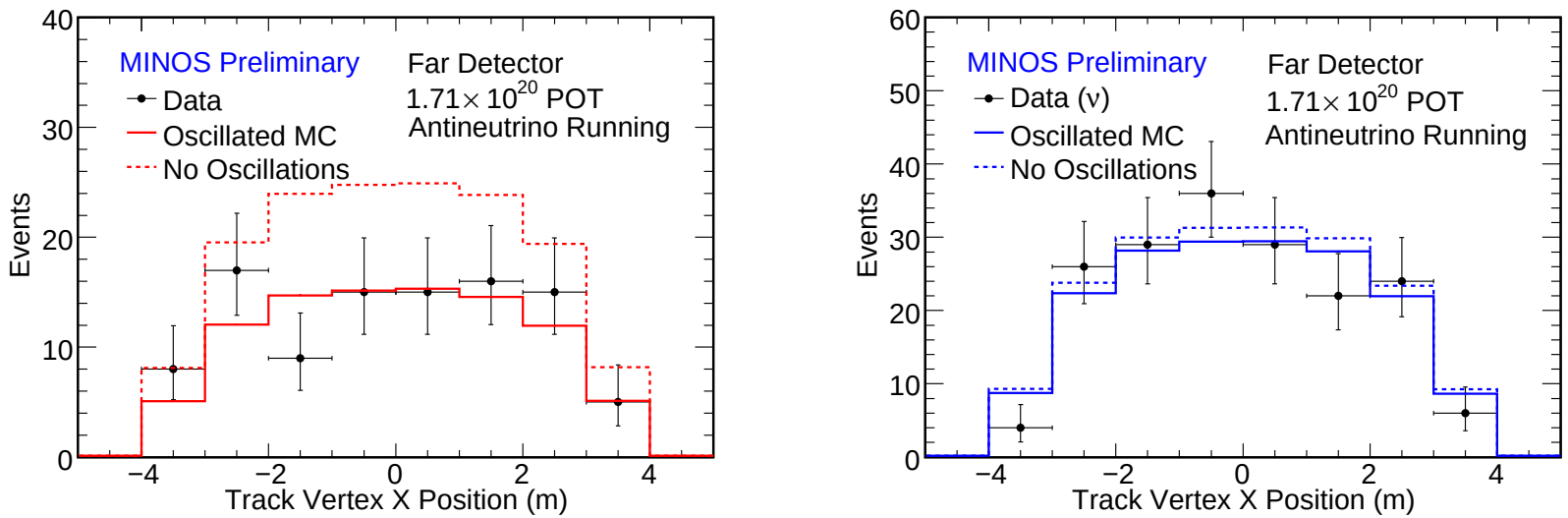

Figure 39: Track vertex X position distribution of selected $\overline{\nu}_\mu$ events (left, red) and ν_μ events (right, blue) in the Far Detector. The solid colored histograms represents the Monte Carlo expectation with the best fit oscillation parameters, the dashed colored histograms represents the no oscillations expectation and black points represent data. MC is pot normalized to data.

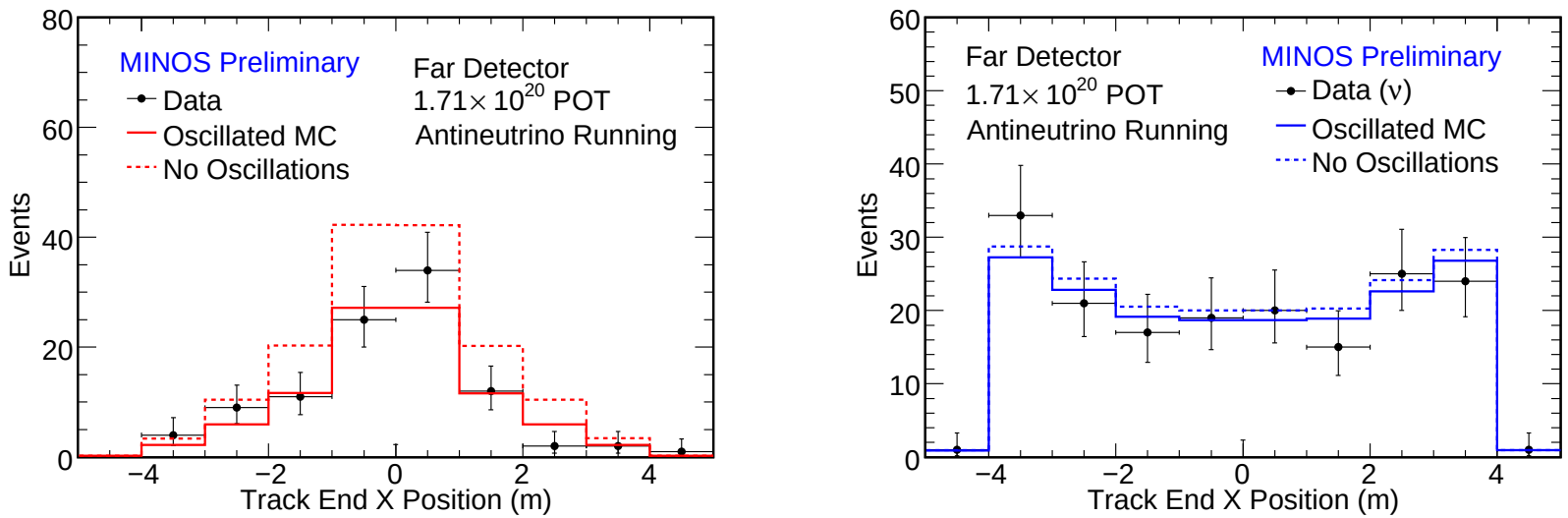

Figure 40: Track end X position distribution of selected $\overline{\nu}_\mu$ events (left, red) and ν_μ events (right, blue) in the Far Detector. The solid colored histograms represents the Monte Carlo expectation with the best fit oscillation parameters, the dashed colored histograms represents the no oscillations expectation and black points represent data. MC is pot normalized to data.

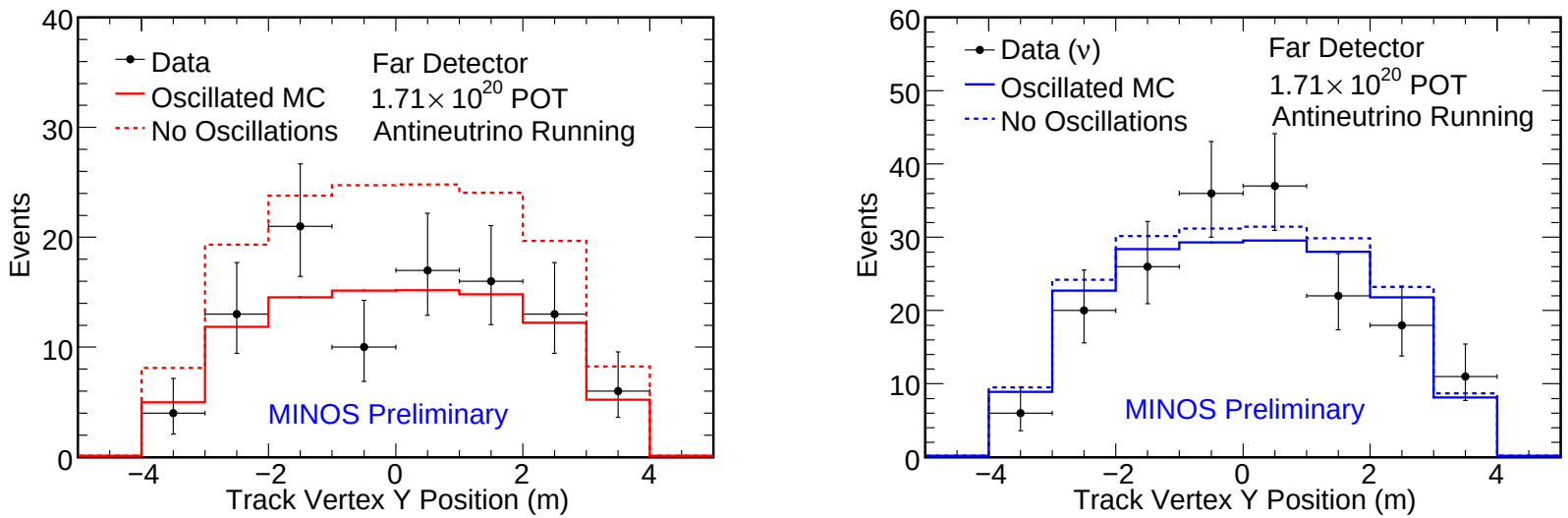

Figure 41: Track vertex Y position distribution of selected $\overline{\nu}_\mu$ events (left, red) and ν_μ events (right, blue) in the Far Detector. The solid colored histograms represents the Monte Carlo expectation with the best fit oscillation parameters, the dashed colored histograms represents the no oscillations expectation and black points represent data. MC is pot normalized to data.

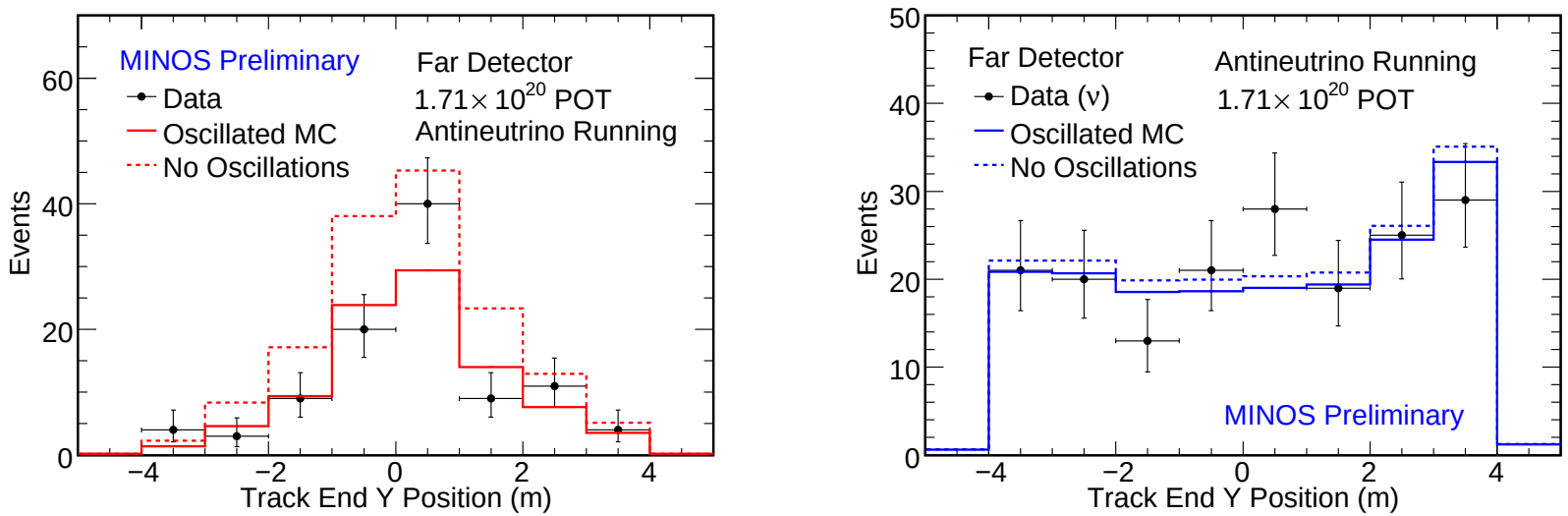

Figure 42: Track end Y position distribution of selected $\overline{\nu}_\mu$ events (left, red) and ν_μ events (right, blue) in the Far Detector. The solid colored histograms represents the Monte Carlo expectation with the best fit oscillation parameters, the dashed colored histograms represents the no oscillations expectation and black points represent data. MC is pot normalized to data.

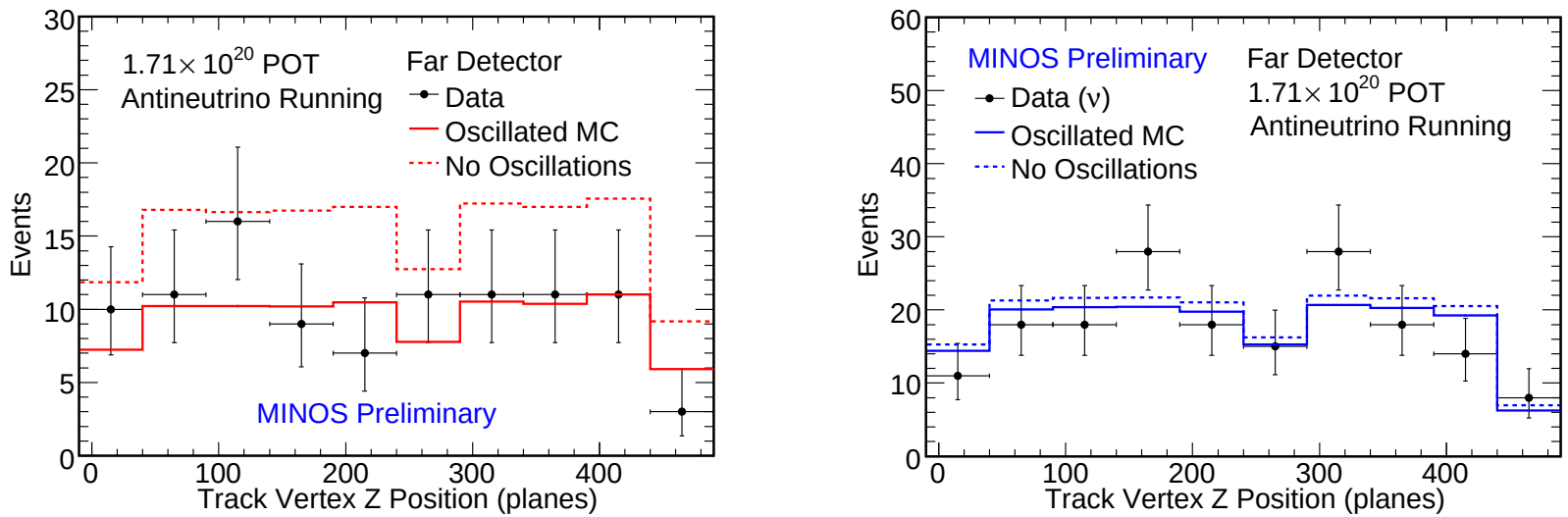

Figure 43: Track vertex longitudinal position distribution of selected $\overline{\nu}_\mu$ events (left, red) and ν_μ events (right, blue) in the Far Detector. The solid colored histograms represents the Monte Carlo expectation with the best fit oscillation parameters, the dashed colored histograms represents the no oscillations expectation and black points represent data. MC is pot normalized to data.

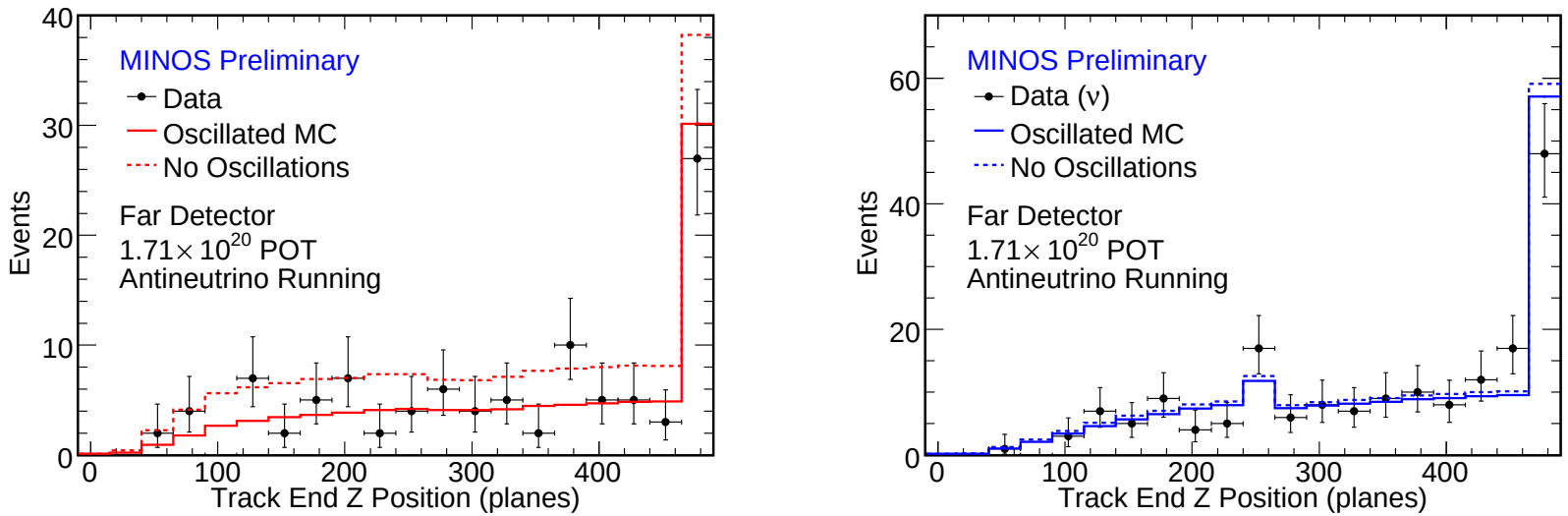

Figure 44: Track end longitudinal position distribution of selected $\overline{\nu}_\mu$ events (left, red) and ν_μ events (right, blue) in the Far Detector. The solid colored histograms represents the Monte Carlo expectation with the best fit oscillation parameters, the dashed colored histograms represents the no oscillations expectation and black points represent data. MC is pot normalized to data.

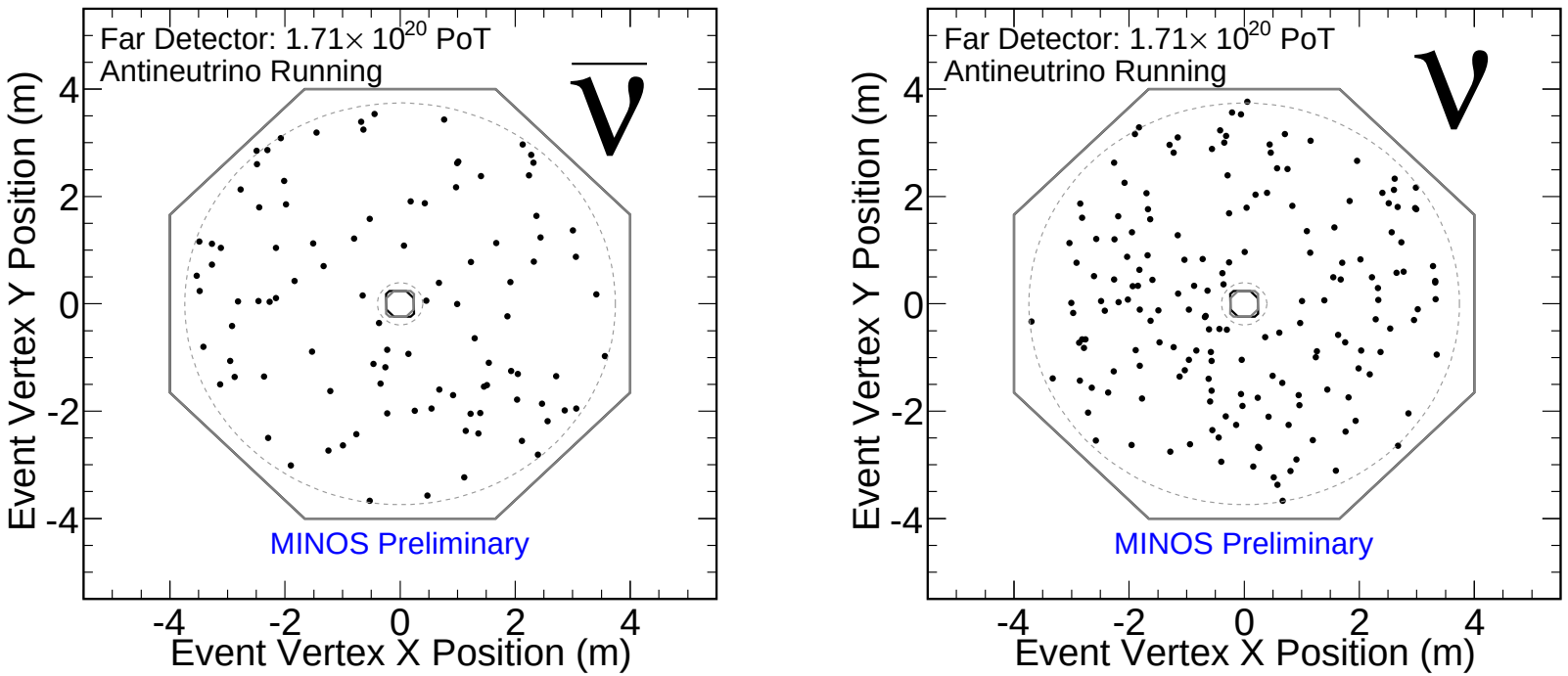

Figure 45: Distribution of track vertex positions in Y vs. X for selected antineutrinos (left) and selected neutrinos (right).

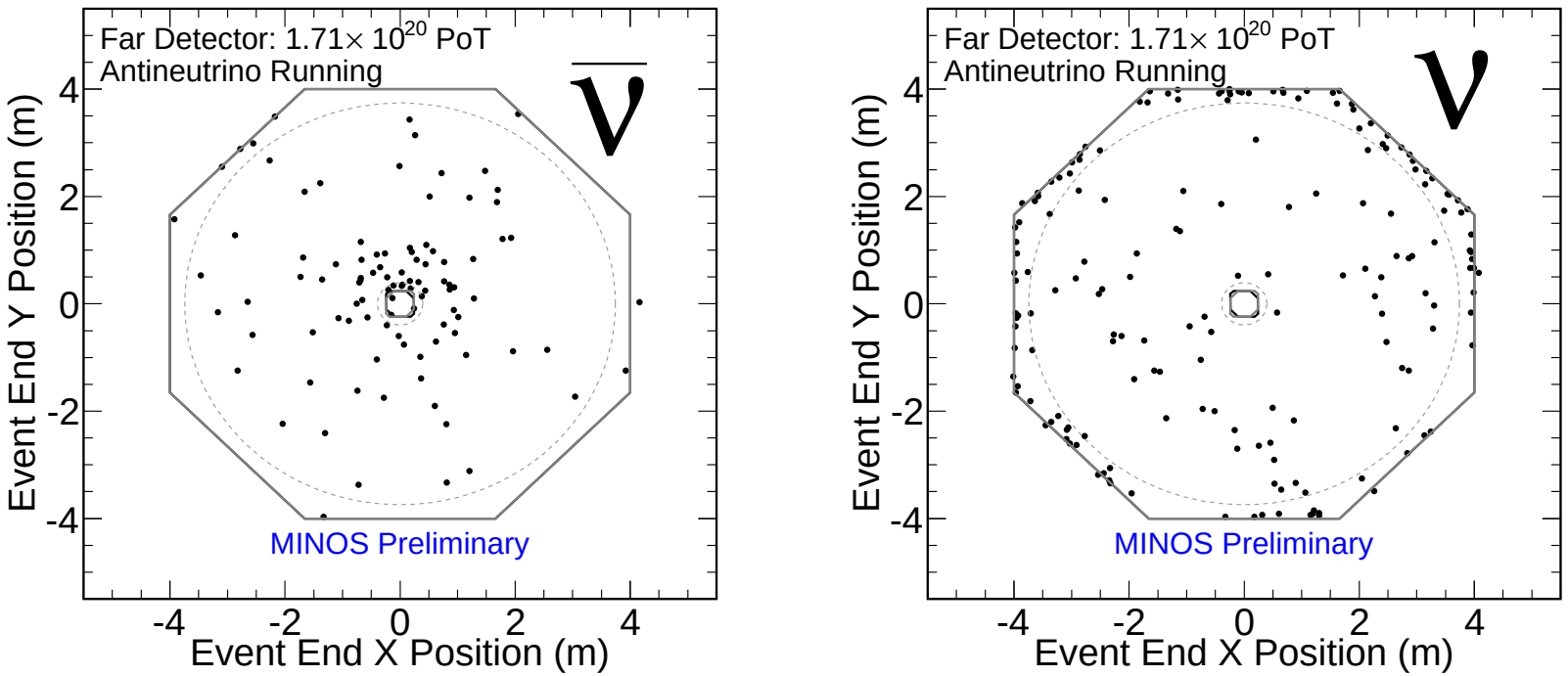

Figure 46: Distribution of track end positions in Y vs. X for selected antineutrinos (left) and selected neutrinos (right).

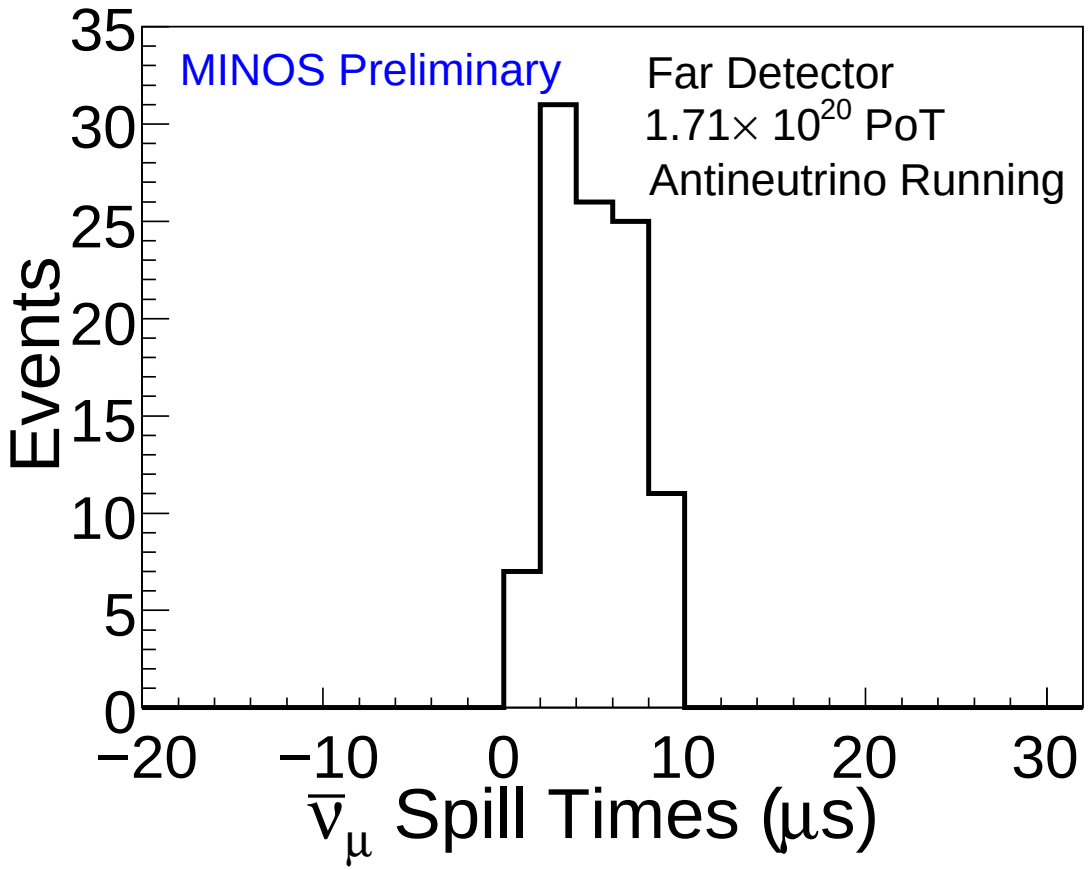

Figure 47: Spill times of selected antineutrino events in the Far Detector. Quality criteria impose a $[-2, 12]\ \mu$s boundary for events to be selected.

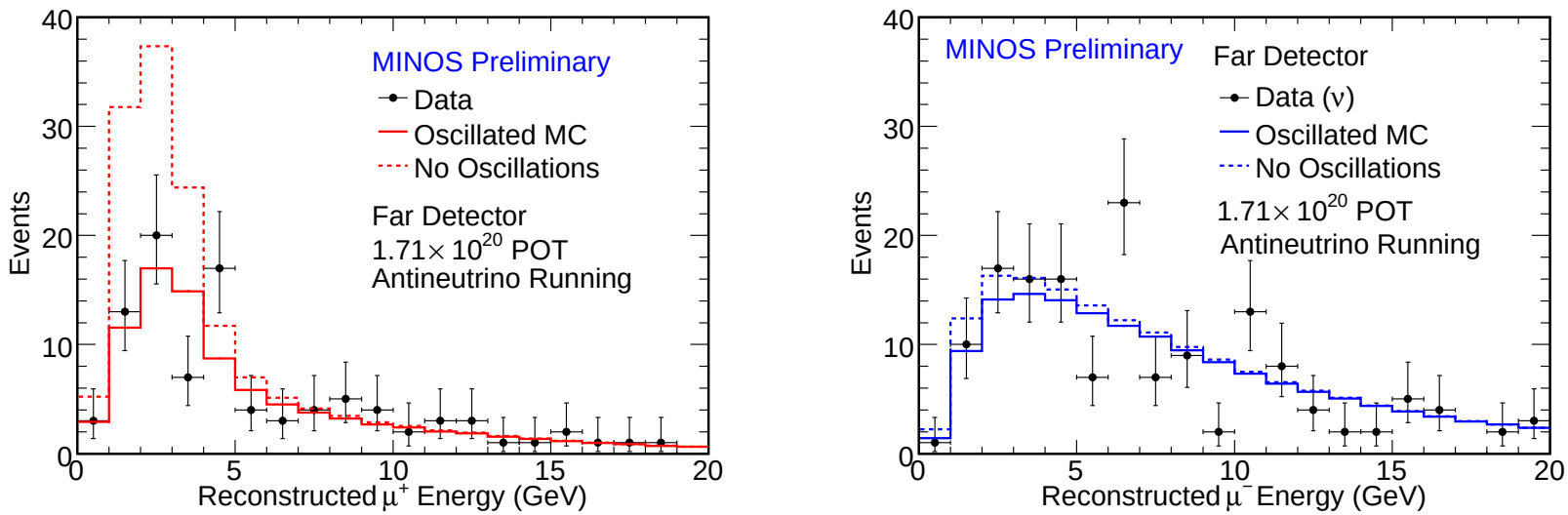

Figure 48: μ^+ track energy distribution of selected $\overline{\nu}_\mu$ events (left, red) and ν_μ events (right, blue) in the Far Detector. The solid colored histograms represents the Monte Carlo expectation with the best fit oscillation parameters, the dashed colored histograms represents the no oscillations expectation and black points represent data. MC is pot normalized to data.

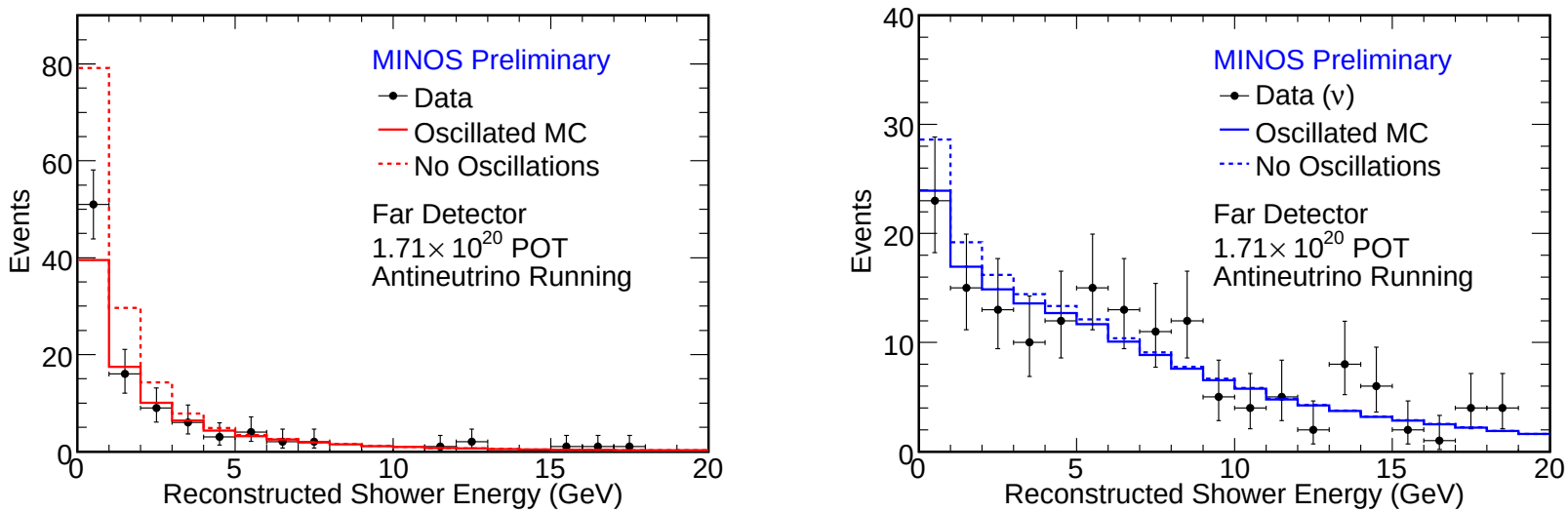

Figure 49: Hadronic shower energy distribution of selected $\overline{\nu}_\mu$ events (left, red) and ν_μ events (right, blue) in the Far Detector. The solid colored histograms represents the Monte Carlo expectation with the best fit oscillation parameters, the dashed colored histograms represents the no oscillations expectation and black points represent data. MC is pot normalized to data.

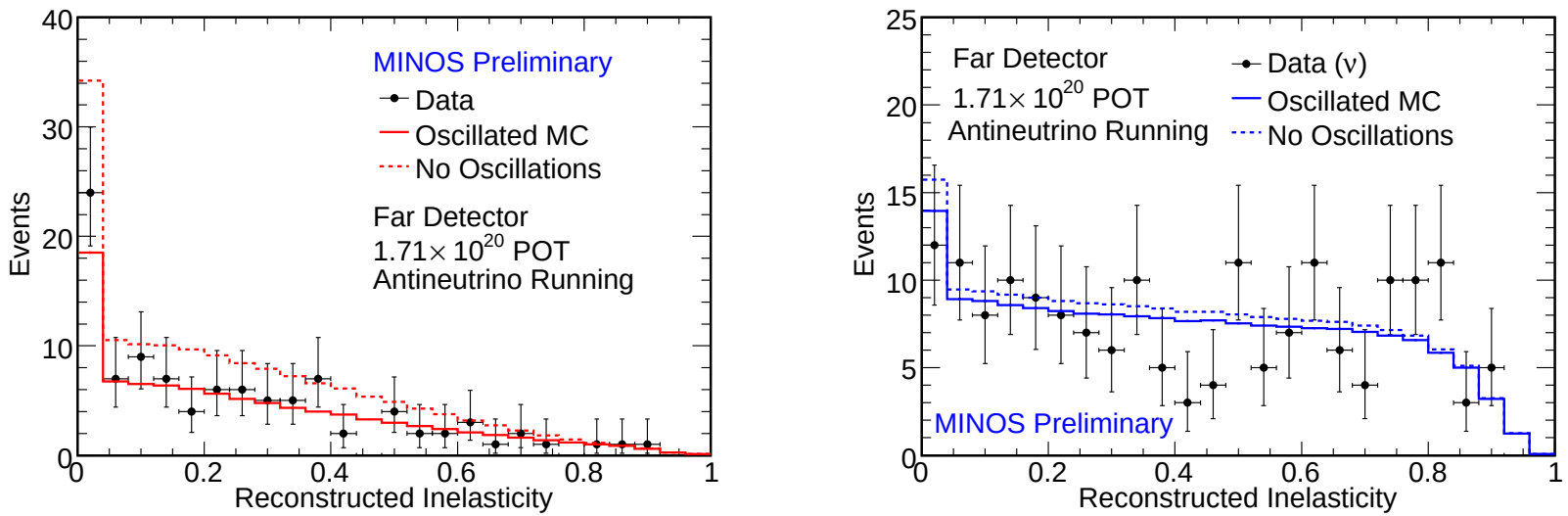

Figure 50: Inelasticity distribution of selected $\overline{\nu}_\mu$ events (left, red) and ν_μ events (right, blue) in the Far Detector. The solid colored histograms represents the Monte Carlo expectation with the best fit oscillation parameters, the dashed colored histograms represents the no oscillations expectation and black points represent data. MC is pot normalized to data.

Extrapolation, Sensitivity, and Systematics

minos-doc-7136

minos-doc-7195

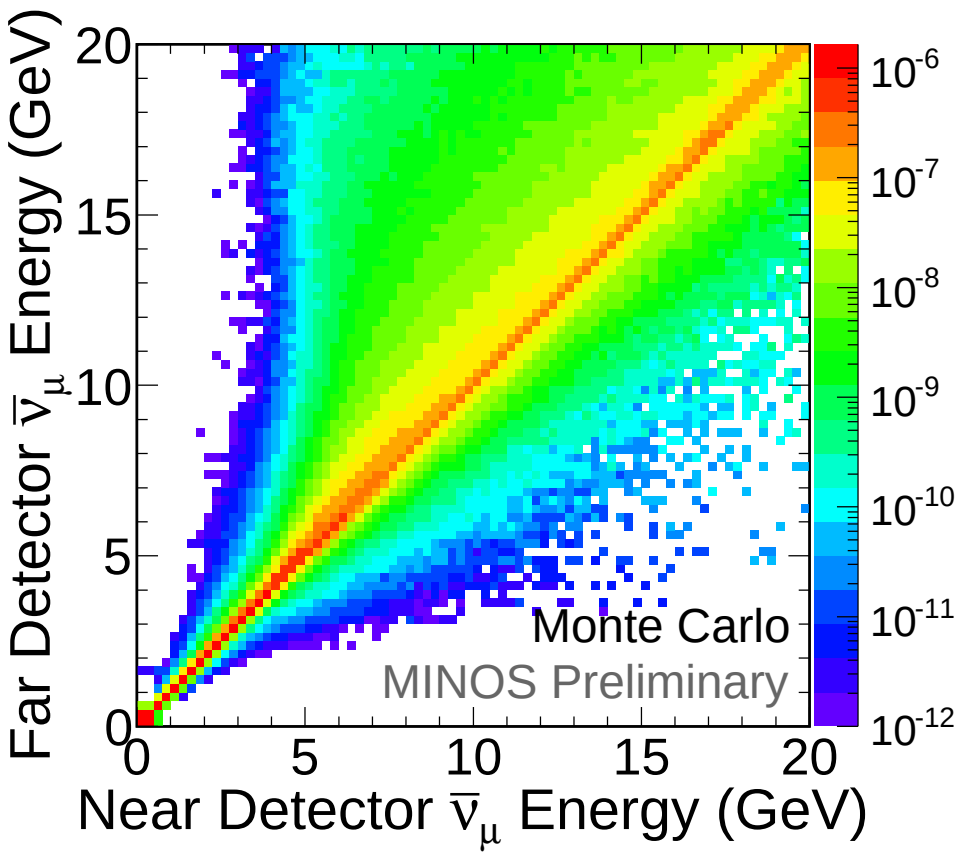

Figure 51: The beam matrix for RHC $\bar{\nu}_\mu$ events. The contents of each cell represent the mean number of $\bar{\nu}_\mu$ events expected in the Far detector for one event in the Near detector. This distribution is treated as a matrix to relate the energies measured in the Near Detector to those in the Far Detector. minos-doc-7136

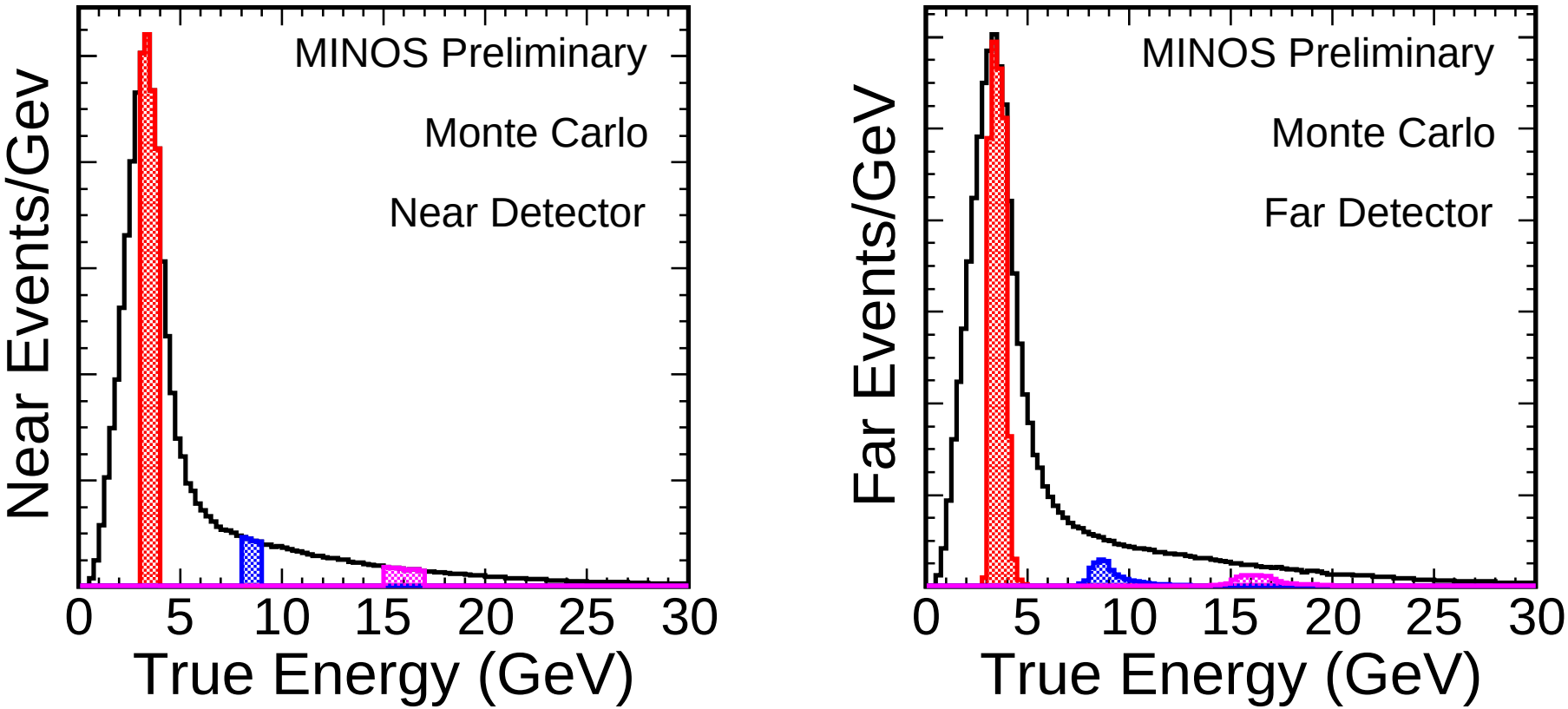

Figure 52: The relationship between the energy of $\bar{\nu}_\mu$ events observed in the Near Detector with those observed in the Far Detector. Decays of $\pi/K/\mu$ producing events of a given energy in the Near Detector would produce a range of energies in the Far Detector, yielding the energy smearing seen here. This is the information encoded in the beam matrix. minos-doc-7136

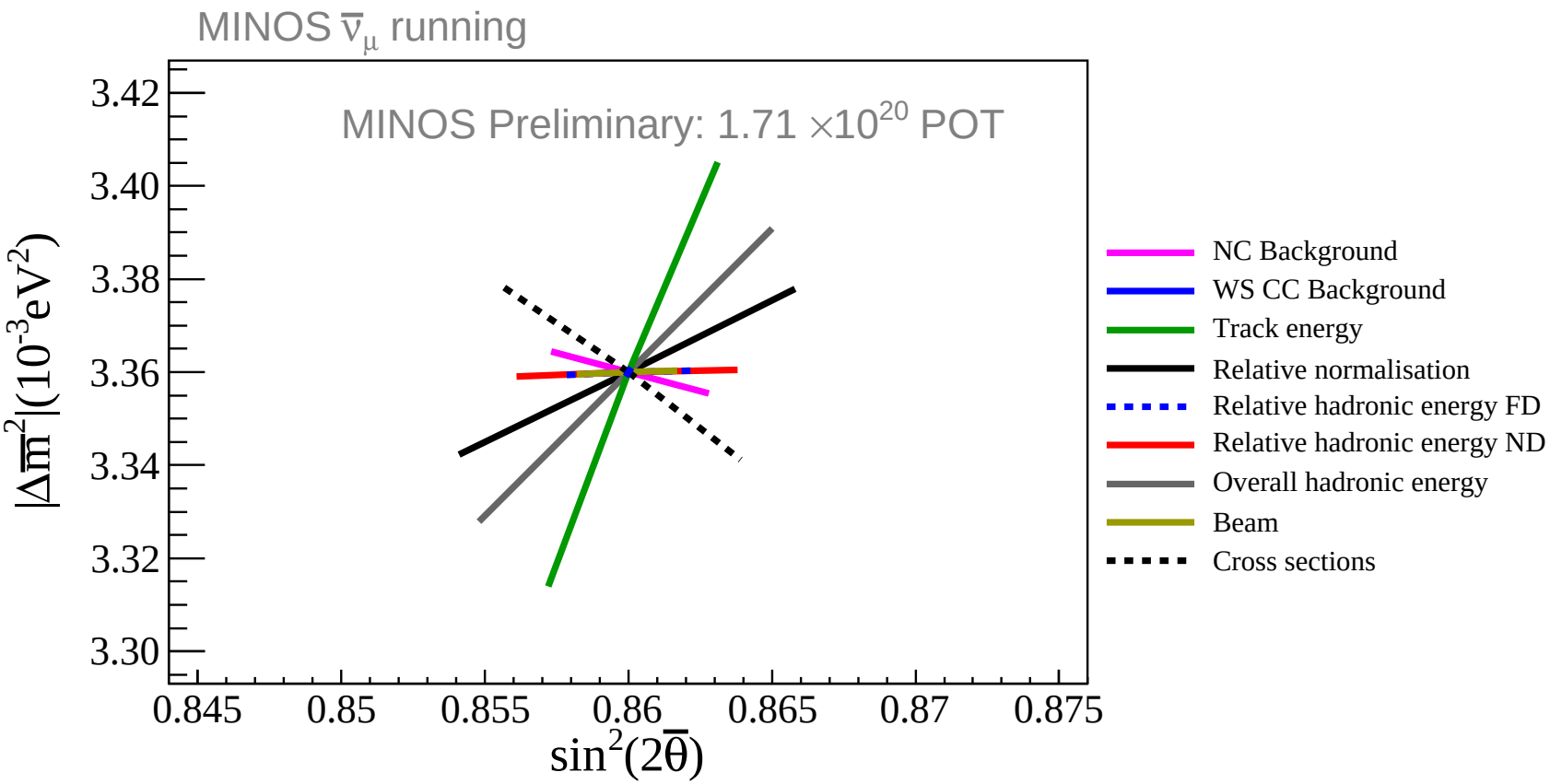

Figure 53: The shifts to the best fit oscillation parameters induced by the application of the 2010 NuMuBar RHC analysis systematic shifts to the fake data. The sum, in quadrature, of all cross section shifts is also shown. minos-doc-7195

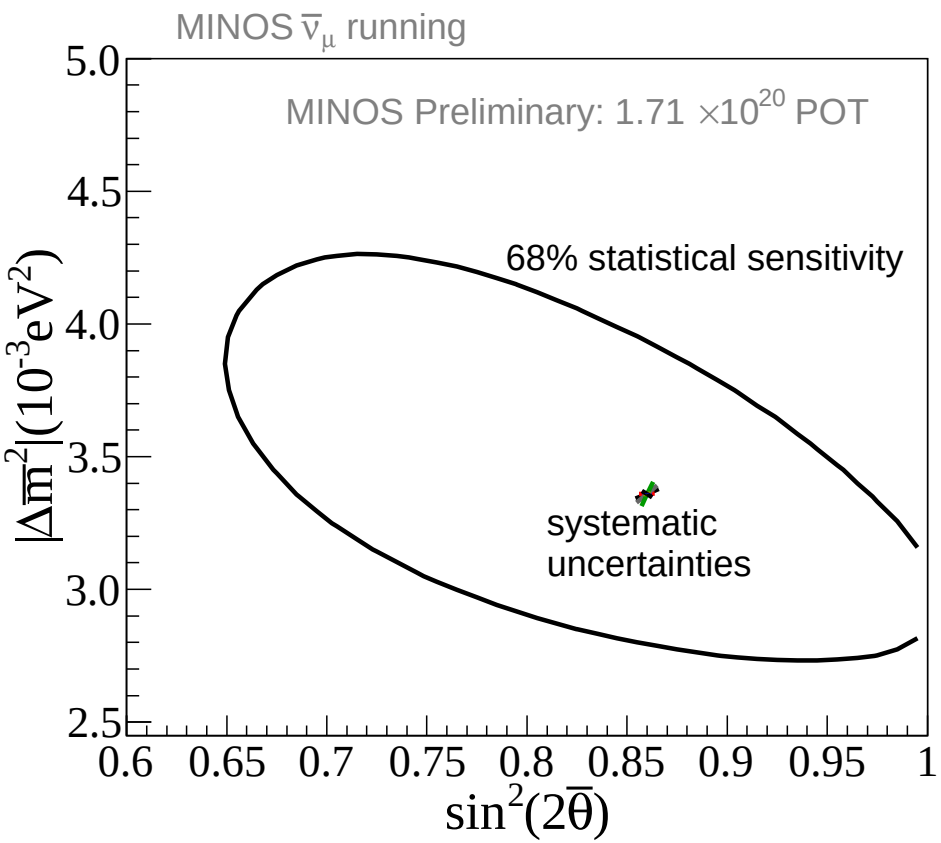

Figure 54: The shifts to the best fit oscillation parameters and the statistical sensitivity contour (black curve). minos-doc-7195

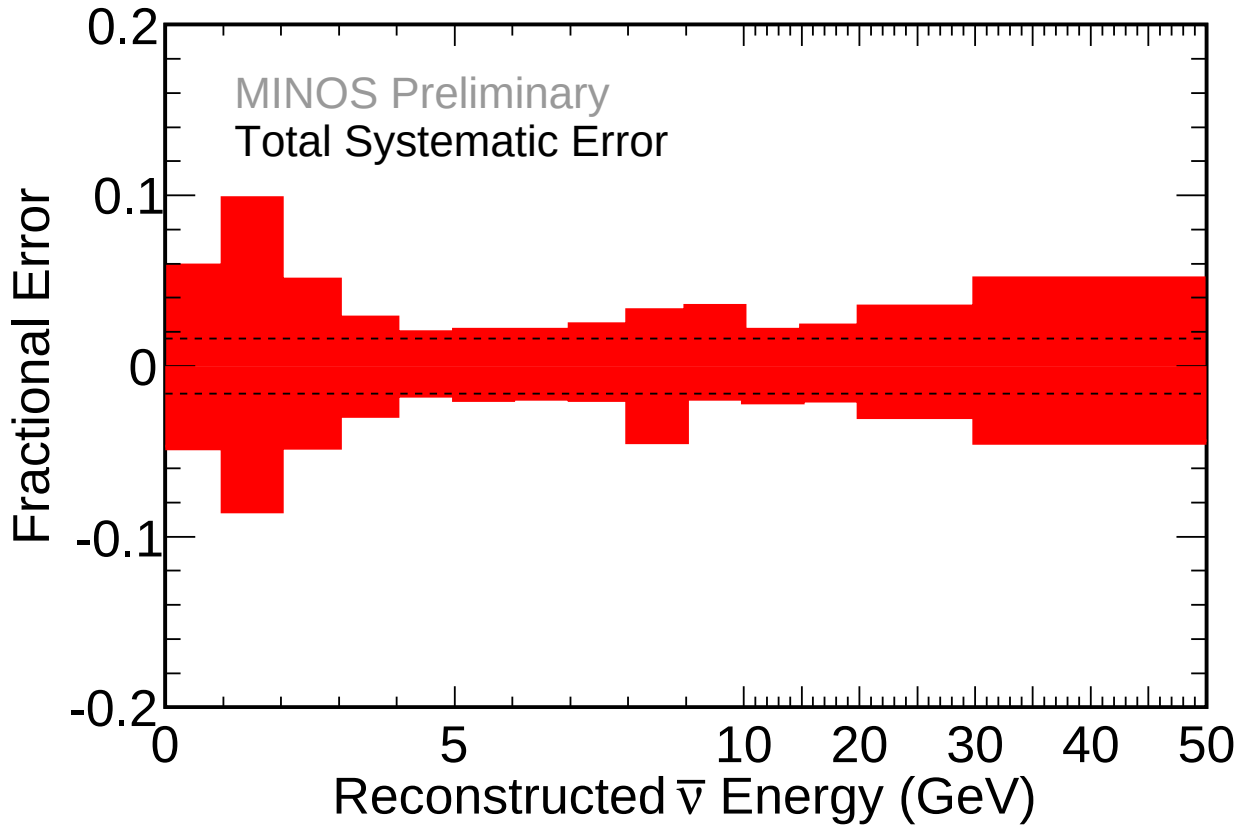

Figure 55: Total systematic error band on the Far Detector prediction. The band is obtained by adding the effect of each individual systematic shift on the FD predicted energy spectrum in quadrature.

Oscillation Results

minos-doc-7246

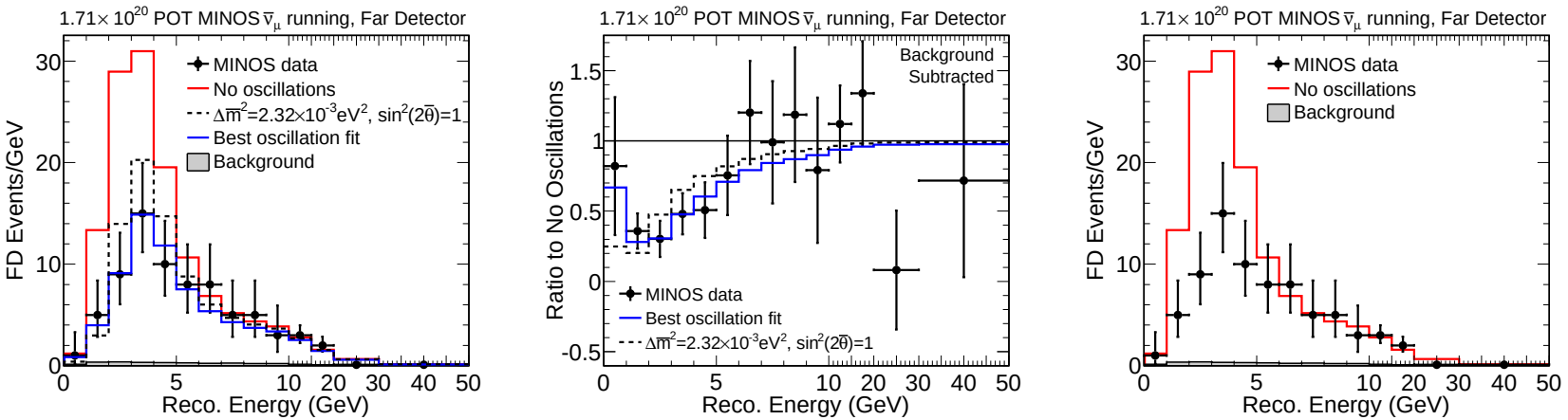

Figure 56: At left the Far Detector data, best fit, cc best fit, and no oscillation prediction. At right are the ratios of data and best fit to the no oscillation hypothesis. The best fit is at $|\Delta\bar{m}^2_{atm}| = 3.36 \times 10^{-3}$ eV^2 and $\sin^2(2\bar{\theta}_{23}) = 0.858$. minos-doc-7246

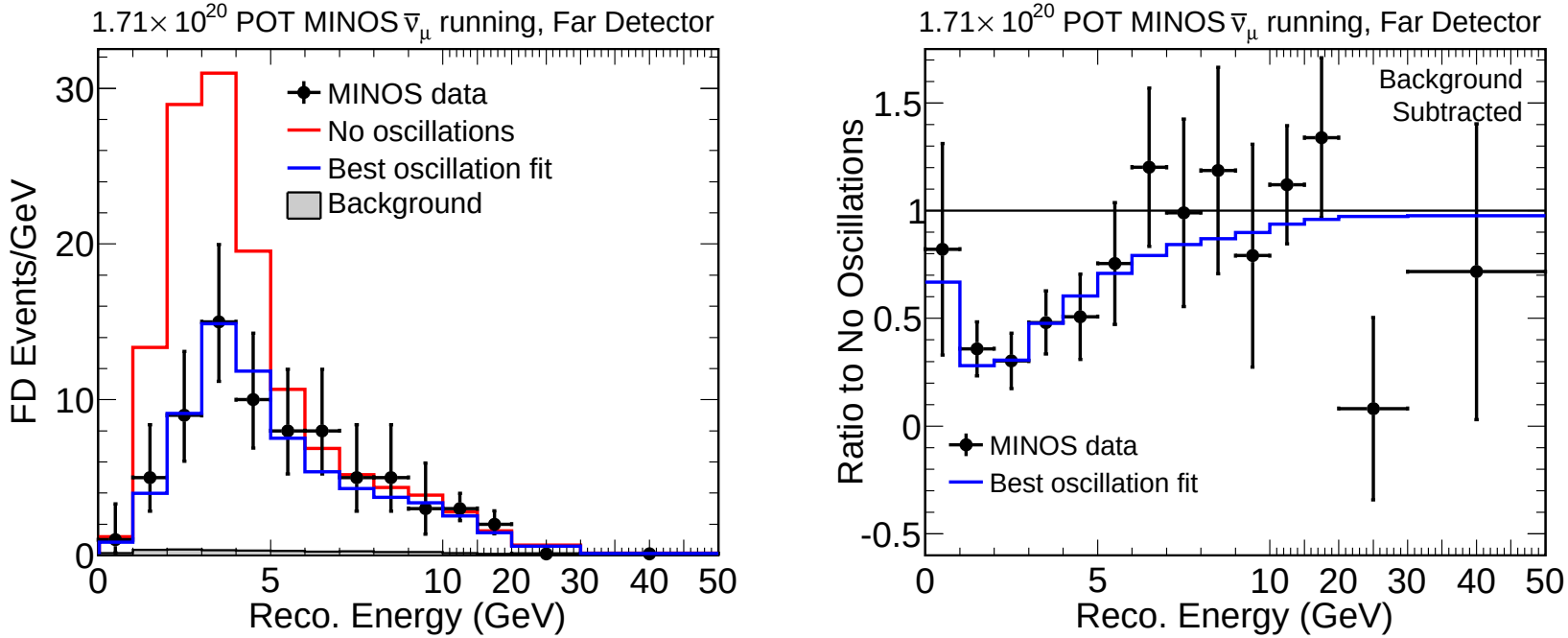

Figure 57: At left the Far Detector data, best fit, and no oscillation prediction. At right are the ratios of data and best fit to the no oscillation hypothesis. The best fit is at $|\Delta\bar{m}^2_{atm}| = 3.36 \times 10^{-3}$ eV^2 and $\sin^2(2\bar{\theta}_{23}) = 0.858$.

We observe 97 events below 50 GeV.
Assuming no oscillations, we would expect 156 events.
Assuming oscillations with the CC neutrino best fit parameters, we would expect 110 events.

Best fit to oscillations

$$|\Delta\bar{m}^2| = 3.36^{+0.45}_{-0.40}\ \text{(stat.)}\ \pm 0.06\ \text{(syst.)}\ \times 10^{-3}\ \text{eV}^2$$

$$\sin^2(2\bar{\theta}_{23}) = 0.860 \pm 0.11\ \text{(stat.)}\ \pm 0.01\ \text{(syst.)}$$

$\Delta\chi^2$ from no oscillations: 6.3σ

When compared with the 2011 CC result, there is a 1.99% probability that the two data sets have the same underlying oscillation parameters. minos-doc-7608

No Oscillations

Energy:	0-6 GeV	6-20 GeV	20-50 GeV	0-50 GeV
Signal:	102.5	38.6	7.6	148.7
Wrong Sign:	0.9	2.9	1.8	5.6
NC:	1.2	0.7	0.1	2.0
Tau:	0.0	0.0	0.0	0.0
Total:	104.7	42.1	9.5	156.3

Best Fit Oscillations

Energy:	0-6 GeV	6-20 GeV	20-50 GeV	0-50 GeV
Signal:	46.0	34.5	7.4	87.9
Wrong Sign:	0.7	2.7	1.8	5.3
NC:	1.2	0.7	0.1	2.0
Tau:	0.2	0.0	0.0	0.3
Total:	48.1	38.0	9.3	95.4

CC 2010 Oscillations

Energy:	0-6 GeV	6-20 GeV	20-50 GeV	0-50 GeV
Signal:	59.1	36.2	7.5	102.8
Wrong Sign:	0.7	2.7	1.8	5.3
NC:	1.2	0.7	0.1	2.0
Tau:	0.1	0.0	0.0	0.2
Total:	61.1	39.7	9.4	110.1

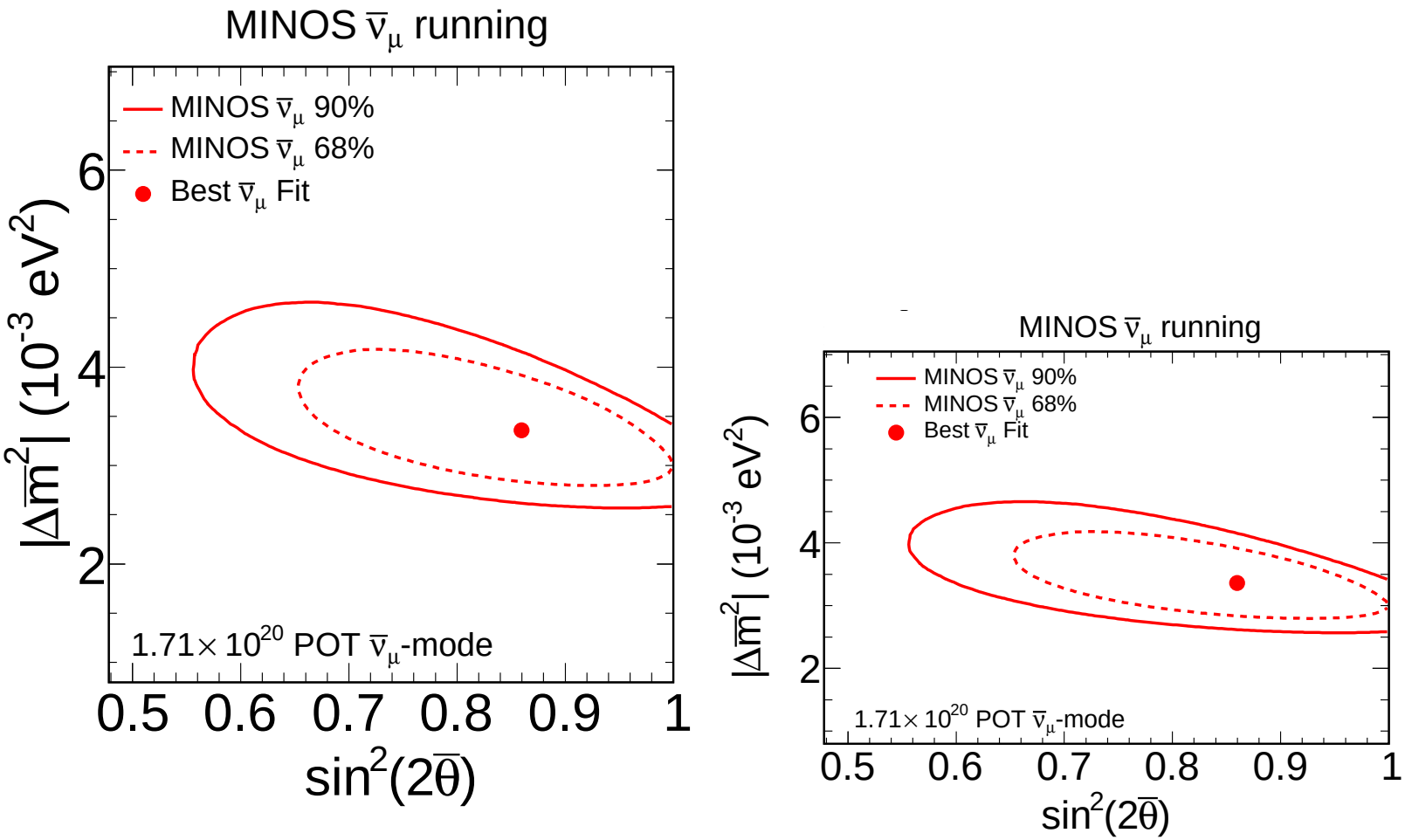

Figure 58: The 68% and 90% antineutrino oscillation contours from RHC running. The contours are determined using the Feldman-Cousins method and include systematics. The best fit is at $|\Delta\bar{m}^2_{atm}| = 3.36 \times 10^{-3}$ eV^2 and $\sin^2(2\bar{\theta}_{23}) = 0.858$.minos-doc-7246

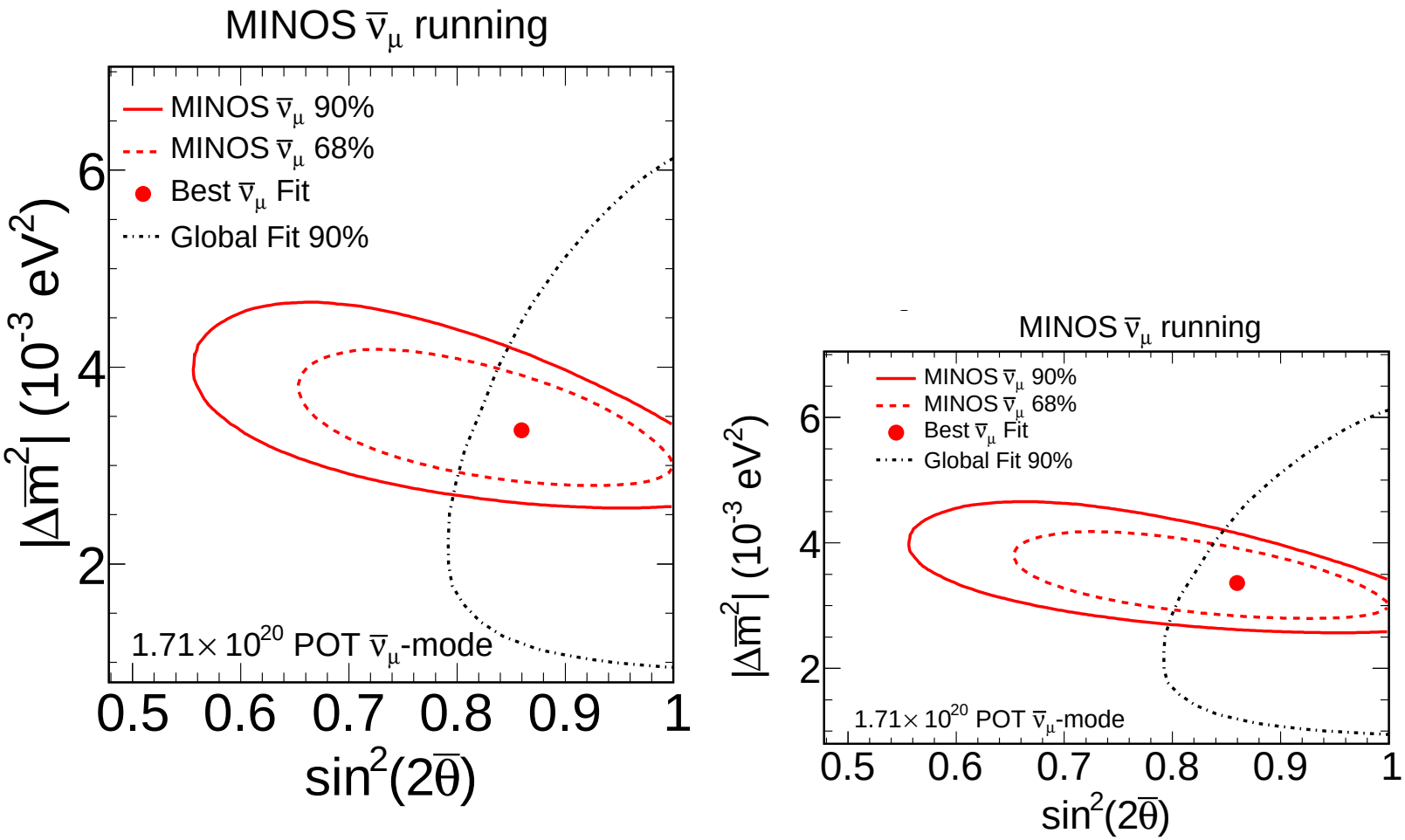

Figure 59: The 68% and 90% antineutrino oscillation contours from RHC running. The contours are determined using the Feldman-Cousins method and include systematics. The best fit is at $|\Delta\bar{m}^2_{atm}| = 3.36\times10^{-3}$ eV^2 and $\sin^2(2\bar{\theta}_{23}) = 0.858$ They are compared with the 90% confidence global fit without MINOS data from M.C. Gonzalez-Garcia and M. Maltoni (Phys. Rept. 460, 2008). minos-doc-7246

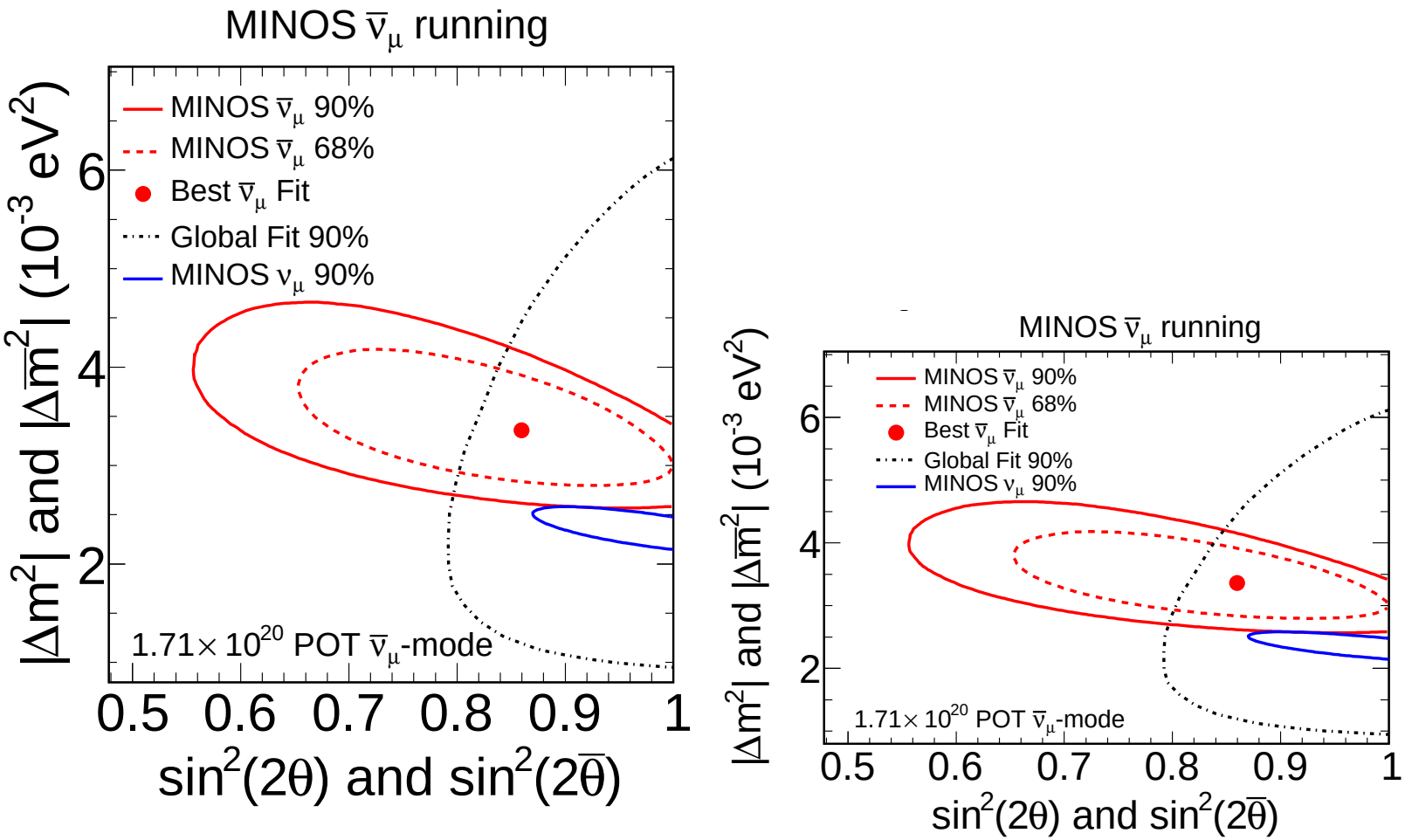

Figure 60: The 68% and 90% antineutrino oscillation contours from RHC running. The contours are determined using the Feldman-Cousins method and include systematics. The best fit is at $|\Delta\bar{m}^2_{atm}| = 3.36 \times 10^{-3}$ eV^2 and $\sin^2(2\bar{\theta}_{23}) = 0.858$. They are compared with the 90% confidence global fit without MINOS data from M.C. Gonzalez-Garcia and M. Maltoni (Phys. Rept. 460, 2008) and the 2010 CC ν_μ result. minos-doc-7246

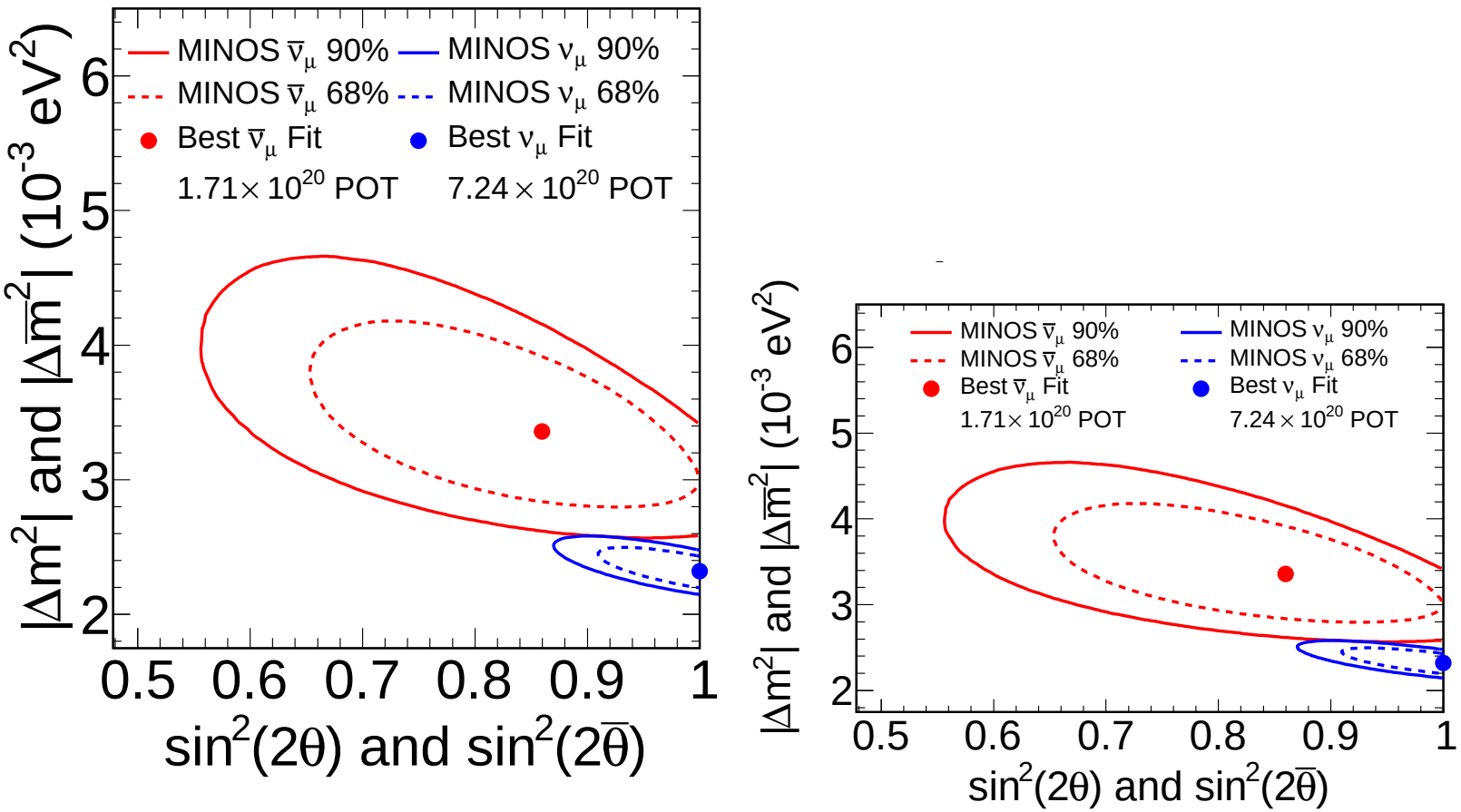

Figure 61: The 68% and 90% antineutrino oscillation contours from RHC running and neutrino oscillation contours from Runs I-III of FHC running. The antineutrino contours are determined using the Feldman-Cousins method and both sets of contours include systematics. The antineutrino best fit is at $|\Delta\bar{m}^2_{atm}| = 3.36\times10^{-3}$ eV^2 and $\sin^2(2\bar{\theta}_{23}) = 0.858$ while the neutrino best fit is at $|\Delta\bar{m}^2_{atm}| = 2.32\times10^{-3}$ eV^2 and $\sin^2(2\theta_{23}) = 1$. minos-doc-7246

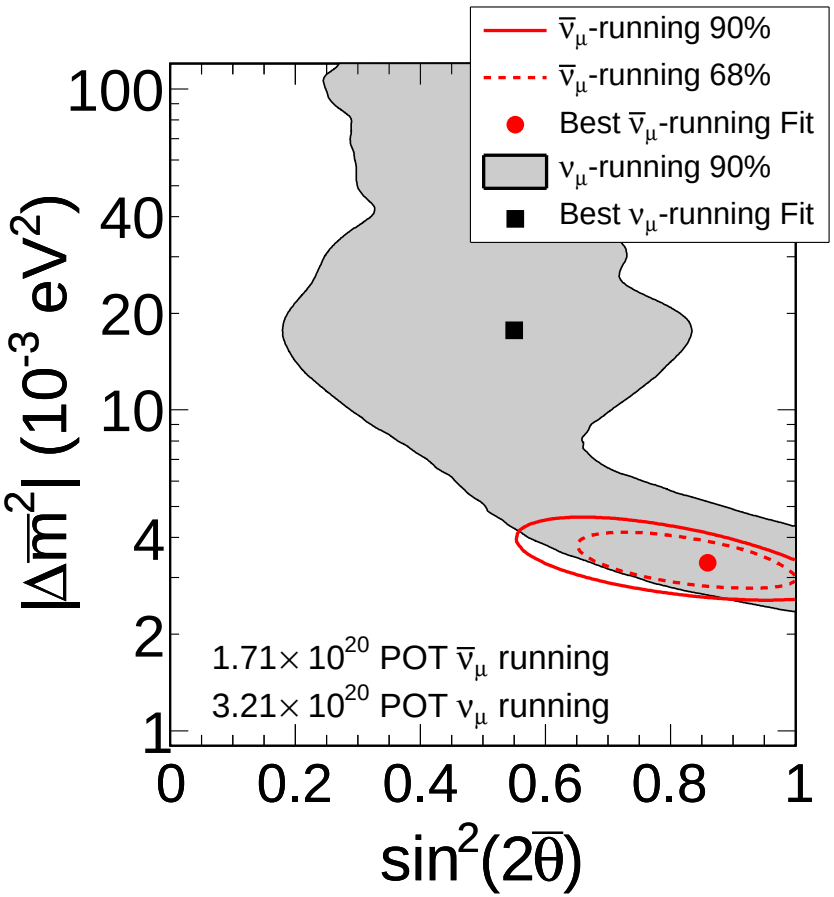

Figure 62: The 68% and 90% antineutrino oscillation contours from RHC running compared with the 90% antineutrino contour from Runs I and II of FHC running. Both sets of contours are determined using the Feldman-Cousins method and include systematics. The best fit for RHC is at $|\Delta\bar{m}^2_{atm}| = 3.36 \times 10^{-3}$ eV^2 and $\sin^2(2\bar{\theta}_{23}) = 0.858$ and the best fit for FHC is at $|\Delta\bar{m}^2_{atm}| = 17.7 \times 10^{-3}$ eV^2 and $\sin^2(2\bar{\theta}_{23}) = 0.55$.

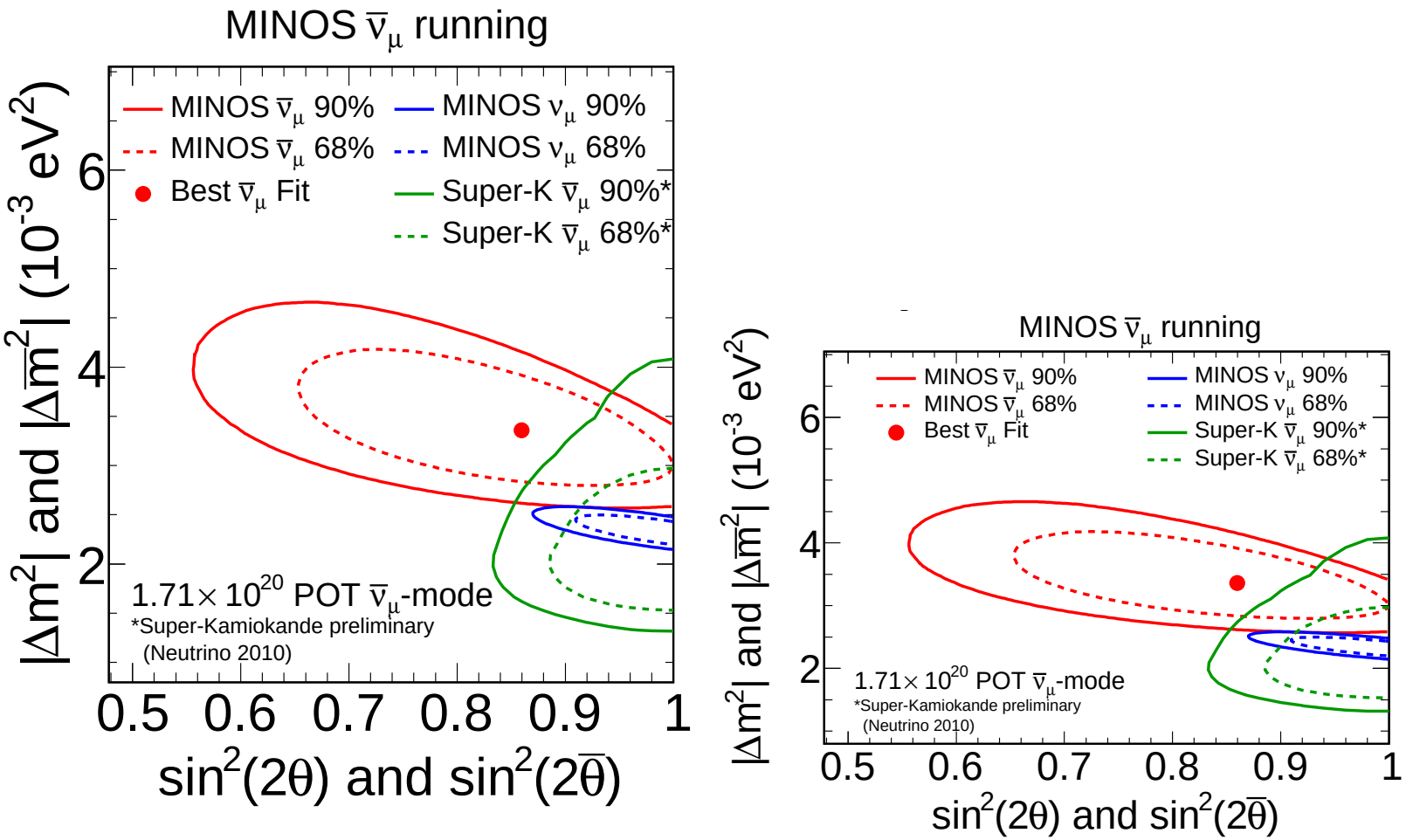

Figure 63: The MINOS antineutrino contours from RHC running. Also showing the MINOS neutrino contours (Runs 1–3, including systematics). Overlayed are the Super-K antineutrino contours presented at Neutrino 2010.

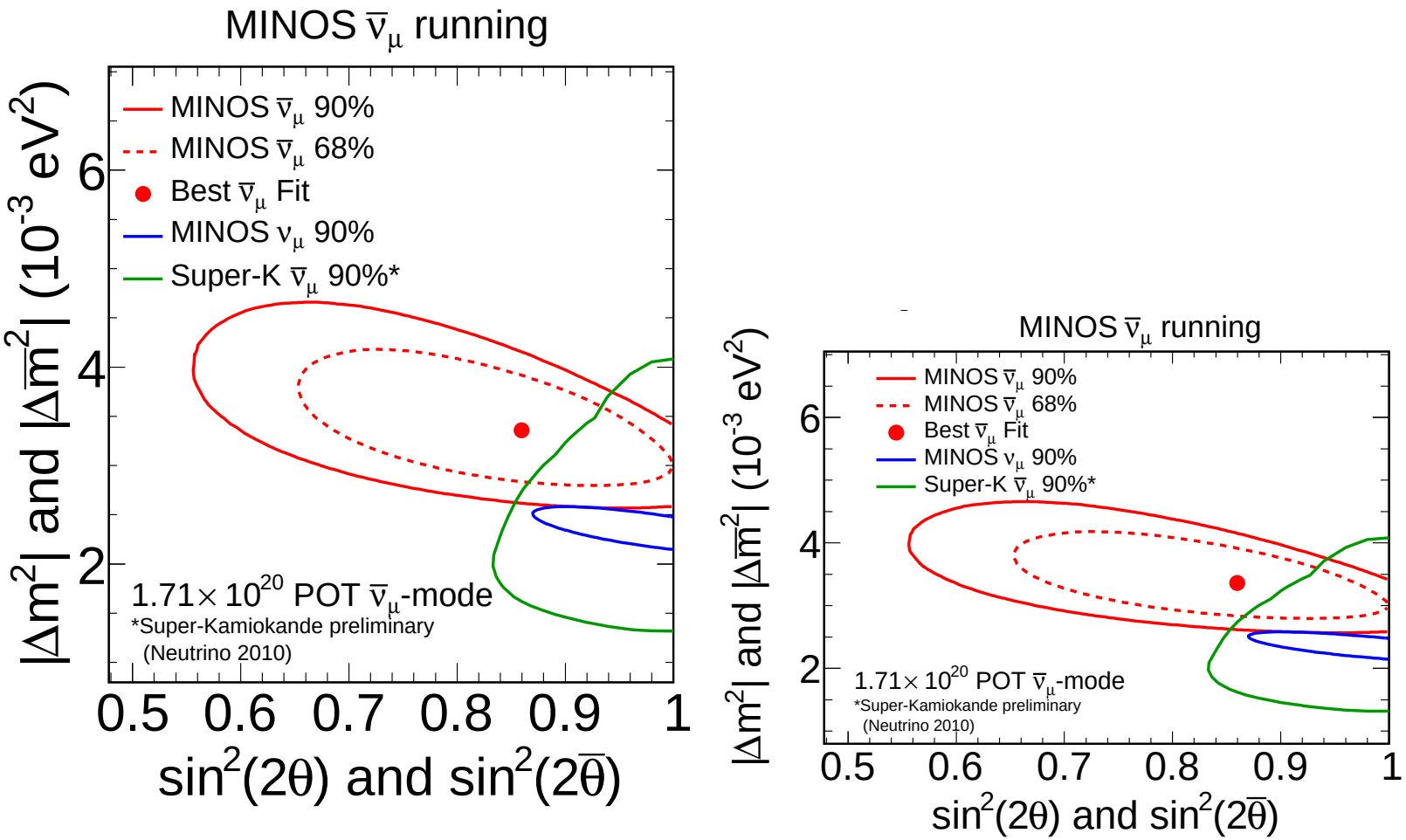

Figure 64: The MINOS antineutrino contours from RHC running. Also showing the MINOS neutrino contours (Runs 1–3, including systematics). Overlayed are the Super-K antineutrino contours presented at Neutrino 2010. (As for the previous slide, but without the numu or Super-K 68% contours to make the plot less busy.)

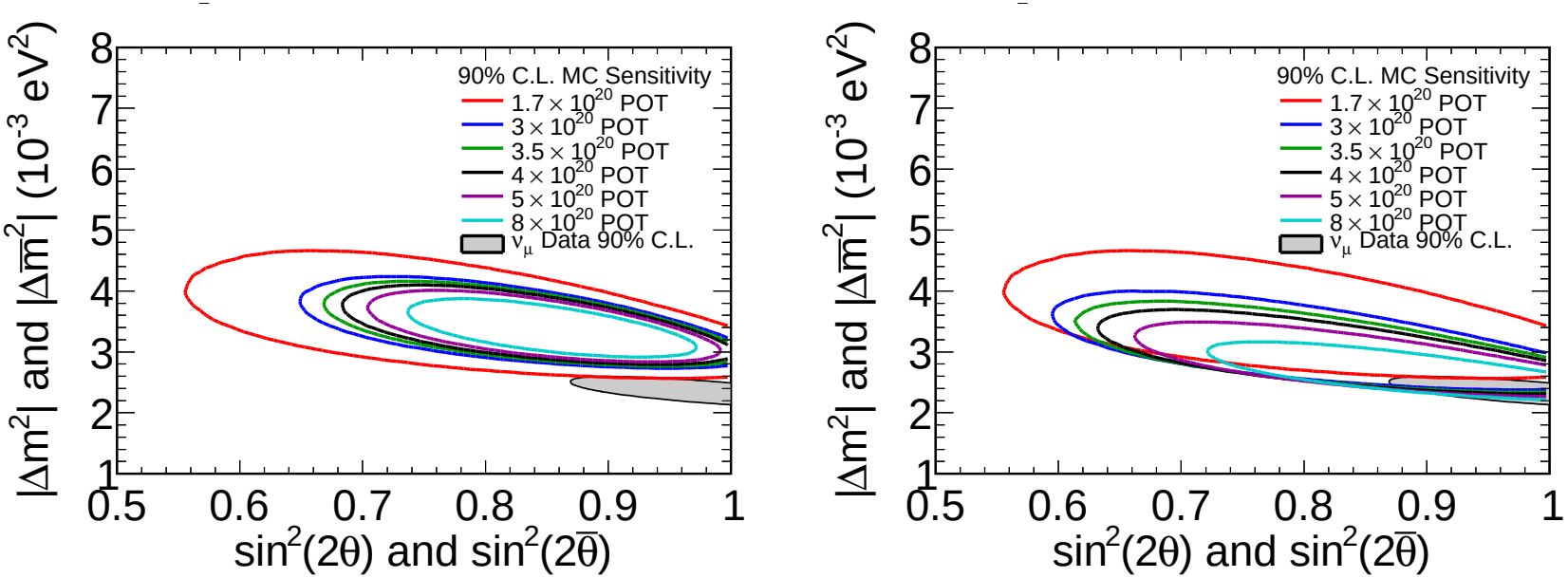

Figure 65: Shown above are the 90% Monte Carlo sensitivities to antineutrino oscillations at a range of NuMI antineutrino beam exposures. The sensitivities are calculated assuming the best fit of the current 1.7×10^{20} POT antineutrino data set (left) $\Delta\overline{m}^2 = 3.36 \times 10^{-3}$ eV^2 and $\sin^2(2\bar{\theta}_{23}) = 0.86$ or the best fit of the 7.2×10^{20} POT neutrino data set for the new data (right) $\Delta\overline{m}^2 = 2.32 \times 10^{-3}$ eV^2 and $\sin^2(2\bar{\theta}_{23}) = 1.0$. Also shown is the 7.2×10^{20} POT MINOS neutrino oscillation result in gray.

PRL Plots

minos-doc-7494

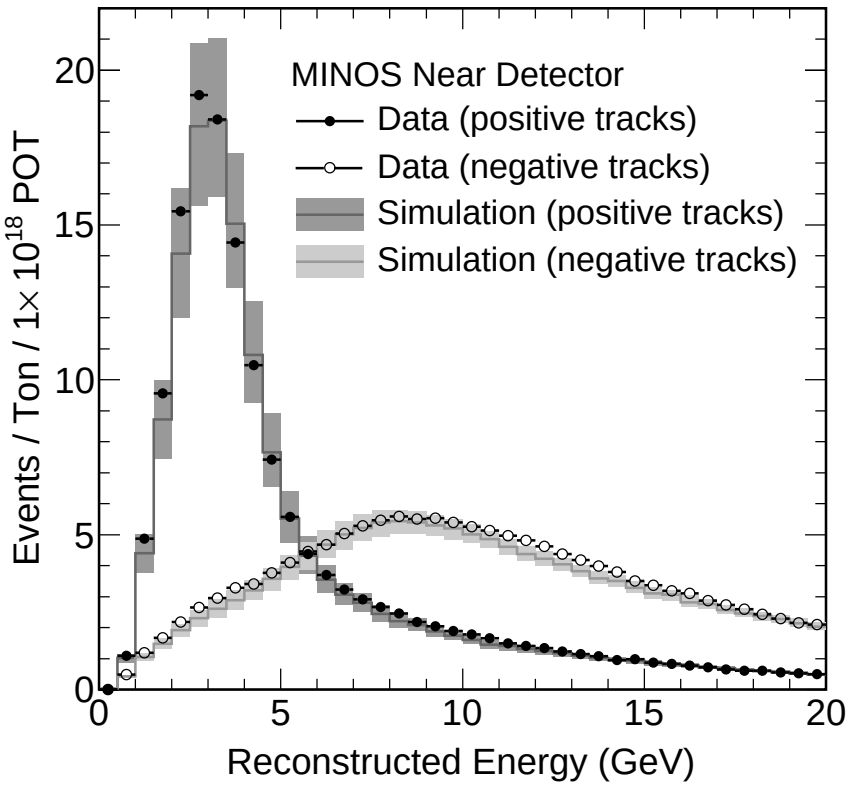

Figure 66: The reconstructed energy spectra of events in the Near Detector classified as charged current interactions. The solid circles show data reconstructed with a positively charged track. The open circles show data reconstructed with a negatively charged track, which are not used in the oscillation analysis. The solid lines show the simulated spectra, with shaded bands representing the systematic uncertainty.

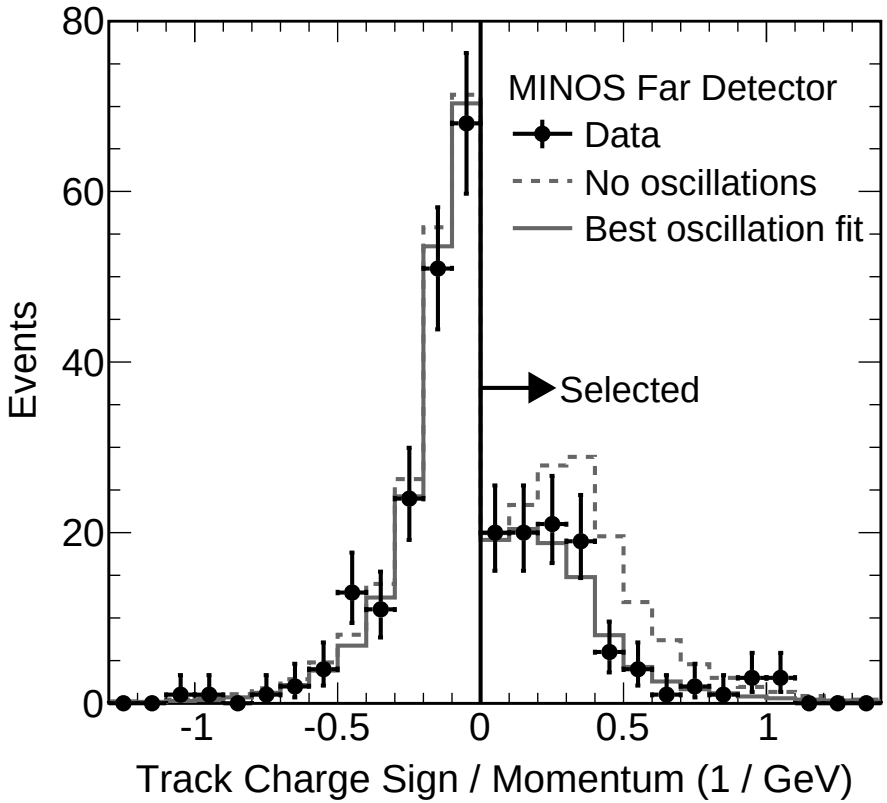

Figure 67: The distribution of the sign of the reconstructed charge divided by the momentum of selected muon tracks in the FD. The simulated distribution is shown in the case of no oscillation, and oscillation assuming the best fit ν_μ parameters from the 2011 CC PRL and $\bar{\nu}_\mu$ parameters from this analysis.

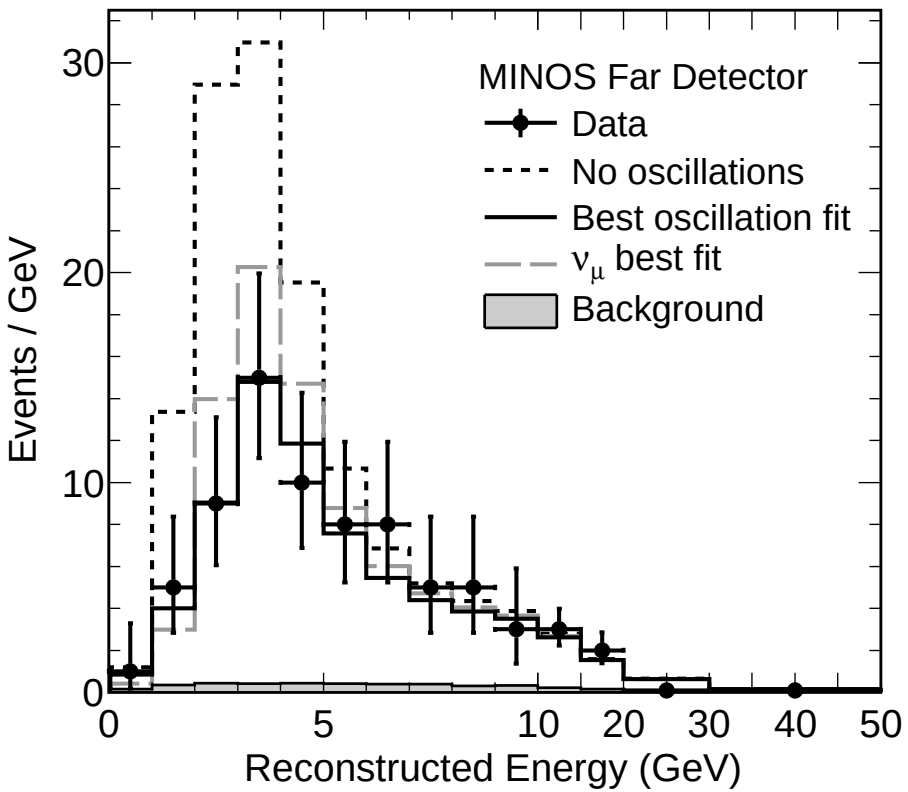

Figure 68: Comparison of the measured Far Detector $\bar{\nu}_\mu$ CC energy spectrum to the expectation in three cases: in the absence of oscillation; using the oscillation parameters which best fit this $\bar{\nu}_\mu$ data (for this case, the total expected background is also indicated); and using the best-fit ν_μ oscillation parameters measured by MINOS.

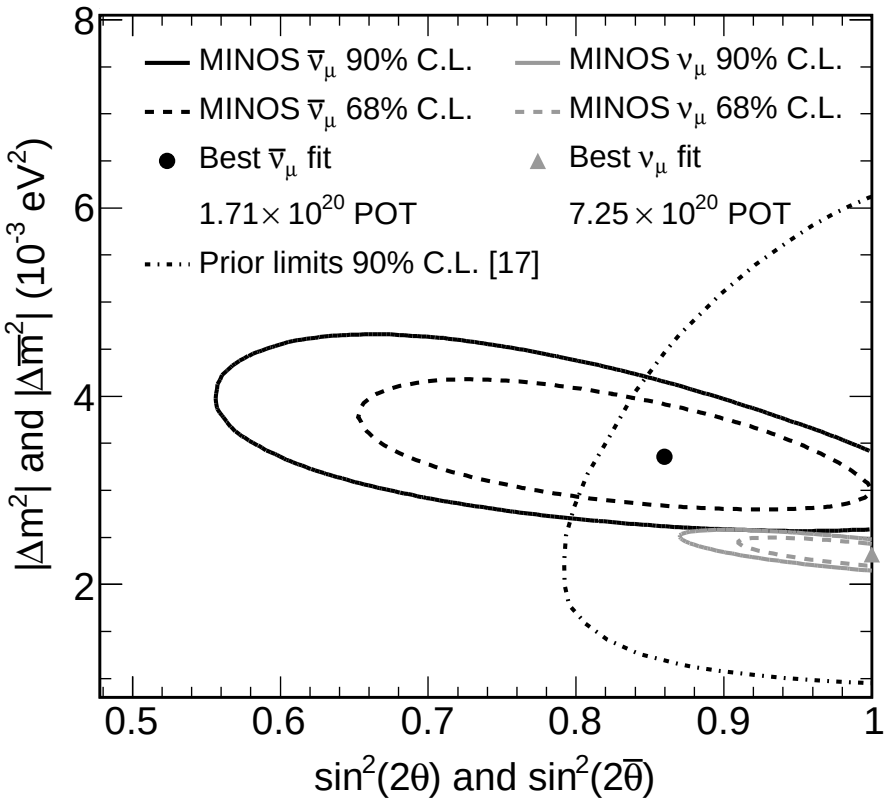

Figure 69: Allowed regions for the $\bar{\nu}_\mu$ oscillation parameters, including all sources of systematic uncertainty. Indirect limits prior to this work [Phys. Rept. **460**, 1 (2008)] and the MINOS allowed region for ν_μ oscillation are also shown.